Journal of Energy Storage 73 (2023) 108849

Contents lists available at ScienceDirect

Journal of Energy Storage

journal homepage: www.elsevier.com/locate/est

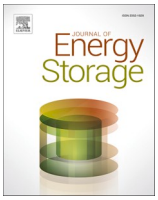

Research papers

Prediction of the discharging time of a latent heat thermal energy storage system with a UA approach

Andreas König-Haagen, Gonzalo Diarce *

ENEDI Research Group, Department of Energy Engineering, Faculty of Engineering of Bilbao, University of the Basque Country UPV/EHU, Bilbao, Spain

ARTICLE INFO

Keywords:
Phase change materials
Latent heat thermal energy storage
Analytical method
Discharging time
Solidification

ABSTRACT

Designing latent heat thermal energy storage systems is a cumbersome task and the estimation of the performance of such a storage system normally involves experiments and detailed numerical simulations. Analytical, empirical and simplified numerical models are much faster but subject to large uncertainties. Even the prediction of the performance of an existing latent heat thermal energy storage system under different boundary conditions is often not possible in an easy way. Therefore, we present an analytical method – the UA approach – to predict the discharging (solidification) time of a flat plate latent heat thermal energy storage system. A special feature of the UA approach is that one can incorporate experimental or numerical results to improve the prediction of the performance under a variety of boundary conditions or material properties. The UA approach was tested for a variation of the Stefan number (Ste), the Biot number (*Bi*), the number of transfer units (NTU) and the heat transfer fluid and was compared to the results of a validated numerical model. The results are promising, especially for small Ste. In addition, the prediction of performance for a high thermal heat conductivity of the phase change material based on a numerical reference solution with a low thermal conductivity worked remarkable well.

1. Introduction

Latent heat thermal energy storage systems (LHTESS) can play a viable role in the transition to a more sustainable energy system. Compared to sensible heat thermal energy storage systems they have a high energy density, especially over narrow temperature ranges. The reason for this high energy density is the phase change – solid/liquid in most cases – that takes place in the phase change materials (PCM) during the charging and the discharging of the LHTESS.

Many PCM have a low thermal conductivity [1] which is considered a major drawback for many applications, since it hinders the rapid charging and discharging of the LHTESS, also called the rate problem [2]. A lot of methods have been developed to overcome this issue [3,4]; however, it is still currently difficult to compare their effectiveness [5–7] and no design rules exist [2]. Even though efforts have been made lately to allow for a comparison of different LHTESS systems under different conditions [5,7] (which will help to develop guidelines for designing LHTESS) or analyzing LHTESS by dividing it into several sections [8], so far either elaborate experiments or detailed simulations have to be carried out to design LHTESS properly. Both are very time-consuming and often expensive, especially if parameter variations are examined.

Analytical approaches, once derived, allow a fast prediction of the charging and discharging time, but are strongly simplified. The analytical approaches are derived from the physical problem and exist for the classical one-dimensional Lamé-Clapeyron-Stefan problem [9,10] and several variants of it [11]. An overview of simplified analytical solutions can be found in Alexiades and Solomon [12], while for close-contact melting one can also find analytical solutions to simplified problems in the literature [13,14]. Another option is empirical correlations, which are available for such cases as melting in a rectangular cavity heated from one side [15] or close contact melting [16,17]. These analytical solutions and correlations, however, cannot be directly applied to LHTESS as they do not include the heat transfer fluid (HTF); they assume constant boundary conditions and do not include the cooling or heating of an HTF, leading to varying boundary conditions along the heat exchange process.

Correlations for the whole LHTESS are often either only valid for a specific design of storage systems or neglect the varying temperature of the HTF along the heat exchanger [18]. The effective-NTU approach – first introduced by Ismail and Goncalves [19] and later applied in

* Corresponding author.
E-mail addresses: andreas_knig001@ehu.eus (A. König-Haagen), gonzalo.diarce@ehu.eus (G. Diarce).

https://doi.org/10.1016/j.est.2023.108849
Received 1 April 2023; Received in revised form 5 August 2023; Accepted 26 August 2023
Available online 17 September 2023

different variants to LHTESS with encapsulated PCM [20,21], tube-in-tank LHTESS [22] and LHTESS with plate design [23] – is a more general approach, but it is still subject to many simplifying assumptions. The first analytical solution that includes the HTF, thus resulting in a quasi-2D model, is based on the quasi-stationary Lamé-Clapeyron-Stefan problem and was used to describe the solidification time of an LHTESS with macro-encapsulated PCM [12]. Later, complex analytical solutions were developed for an LHTESS in plate design, which in practice rely on computations made on a PC [24,25]. Raud et al. [26] presented a model for an LHTESS with a finned heat exchanger based on the solution for a finned isothermal heat exchanger [27]. This model was developed independently, but similar assumptions like in Alexiades and Solomon [12] are made. The same holds for a recent model for different designs of LHTESS [28]. A comprehensive overview of analytical models describing LHTESS can be found in a recent review paper [29].

We herein present a method that aims to predict the discharging (solidification) time of a flat plate LHTESS and thereby its mean discharging power. The method is similar to that presented by Alexiades and Solomon (see chapter 3.5 E in Alexiades and Solomon [12]), but is not based on the splitting of the LHTESS into a discrete number of macro-capsules. Instead, an LHTESS with plate geometry is studied and the method is extended to incorporate numerical or experimental results. This is of great interest from a practical point of view, as it may allow the number of simulations or experiments needed during the design process to be drastically reduced. In addition, we present an equation for the discharging time as a function of an NTU or a UA value, which enables an easy inside into the influence on the LHTESS performance.

To achieve the above-mentioned points, a UA value was calculated based on simplifying assumptions. The method was then tested for a simple LHTESS geometry for a variety of boundary conditions and compared to the results of a validated numerical model for the following situations:

- Predict the LHTESS performance based on material properties, the LHTESS geometry and boundary and initial conditions.
- Based on one numerical or experimental result and a few material properties, the LHTESS performance is predicted for a boundary condition variation or a variation of material properties

2. Case study

The case studied is the solidification process of an LHTESS in plate design. A schematic view of the LHTESS can be seen in Fig. 1. The dimensions of the storage are shown in Table 1. The PCM properties used were generic, but based on actual materials and they are listed in Table 2. Some property values were changed for the different cases studied. The initial and boundary conditions were varied as well and can be found in Table 3. Air and water were used as HTF. Overall, the variations that were performed were to attain different values for representative dimensionless numbers, such as Ste, *Bi*, and NTU, as well as different HTF and operating conditions.

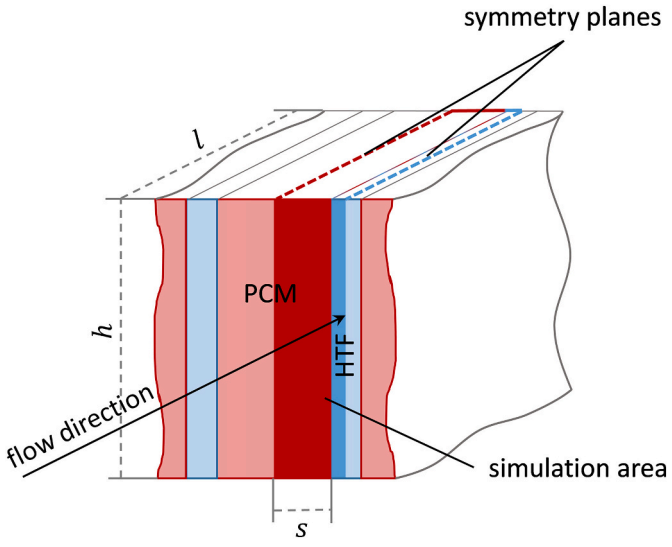

Fig. 1. Scheme of the simulation domain of the LHTESS.

The LHTESS was simulated with a validated numerical model to obtain reference solutions for the developed UA approach. These reference solutions are used as a benchmark to check the accuracy of the UA approach and to give input results for estimating the UA values (see description in Section 3.3) for predicting the LHTESS performance under different conditions.

The numerical model is based on the apparent heat capacity method and uses an automated time step control to prevent over-jumping of the phase change range. The phase change is smoothed with the help of an error function. Heat losses and convection in the PCM are neglected. The used apparent heat capacity method was validated for a one-dimensional test case for a broad range of parameters (time step size, number of nodes and melting range width). The method is rather computational expensive, but showed a sound agreement with the analytical solution. [30]

The overall two-dimensional numerical model was tested for different geometries and boundary conditions against experimental results [7,31]. Moreover, the high agreement of the results of the numerical model with the results of the UA approach for low Ste can also be understood as a validation (see e.g. Fig. 4). In this work a mesh with 420 nodes was used.

3. UA approach

The basis of the UA approach is similar to the method presented in Alexiades and Solomon (ref [12], chapter 3.5 E) to calculate the discharging time of an LHTESS with PCM macro-encapsulated in cylindrical capsules. For the derivation of our method, the LHTESS heat transfer configuration was considered to be quasi-two-dimensional and divided into a certain number of cells in the flow direction of the HTF. This provides a similar picture to the discretization commonly applied in numerical methods, as shown in Fig. 2.

The main idea of the approach is to study one cell after another, following the flow direction of the HTF. The details of the procedure are provided in Sections 3.1 to 3.3. Two different types of approach were developed. They differ in the way the heat transfer resistance in the HTF towards the PCM is treated; the first approach neglects the resistance, while the second one accounts for it. The main assumptions underlying both approaches are outlined below:

- The LHTESS is considered to be quasi-two-dimensional.
- Heat conduction takes place only perpendicular to the HTF flow direction.
- The HTF exhibits plug flow.
- The heat transfer process in the PCM is assumed to be quasi-stationary – the sensible heat is neglected in the heat transfer process. However, a certain amount of sensible heat can be added to the latent heat to account for the energetic effect of the sensible heat.

Table 1
Dimensions of the LHTESS.

Dimension	Value	Unit
l	4.0	m
h	0.5	m
s	0.05	m

Table 2
Material properties of the generic PCM.

Material property	Value	Unit
ρ	1000	kg/m^3
λ	0.1 … 2.0	W/(mK)
c	2000, 200	J/(kgK)
L	200,000, 1[a]	J/kg

[a] A value of 1 J is used to avoid any possible numerical difficulties with 0.

Table 3
Initial and boundary conditions and some dimensionless numbers of the LHTESS.

Condition	Value	Unit
T_{in}^{LTES}	332	K
T_{init}	352	K
T_m	342	K
$\dot{m}$	Air: 0.1 … 10	kg/s
	Water: (0.1…10) • c_p^{air}/c_p^{water}[a]	
k	1000, 100	W/(m^{2}K)
Ste	0.02 … 40,000	
Bi	2,5 … 500	

[a] c_p^{air}/c_p^{water} is used to get the same capacity flow for both HTF.

- The PCM properties (except for the melting enthalpy) and those of the HTF are independent of temperature.
- The influence of natural convection is neglected, which is a common assumption during solidification [18].
- The heat transfer process can be described with temporal mean values (e.g., the HTF inlet temperature). Thus, the cells of the LHTESS (see Fig. 2) can be treated separately, one after another.
- After one cell has finished the phase change, no more heat transfer takes place in this cell. Consequently, the inlet temperature of the next cell is the inlet temperature of the LHTESS.

Both approaches (including and neglecting the thermal resistance within the HTF) can also be used to estimate a UA value from numerical or experimental results, which is later used to predict the LHTESS performance for different operation conditions. As a result, four approaches were assessed, whose identifiers are presented in Table 4.

3.1. Neglected heat transfer resistance in the HTF (UA approach 1a)

For this case, we assume that the heat transfer in the HTF towards the PCM is negligible, i.e., $Bi \gg 1$. In this case, the solidification time of the first cell t_{sol}^{init} can be described by Eq. (1) [12]:

$$t_{sol}^{init} = \frac{1}{2} \bullet \frac{L \bullet \rho}{\lambda \bullet \left(T_m - T_{in}^{LTES}\right)} \bullet s^2 \tag{1}$$

Here, the melting enthalpy is L, the density and heat conductivity of the PCM are ρ and λ, while the thickness of the PCM layer is s (see Fig. 1). The melting temperature of the PCM is T_m and the inlet temperature of the HTF in the LHTESS is T_{in}^{LTES}. The mean power $\overline{\dot{Q}}$ can be calculated for any cell with Eq. (2)

$$\overline{\dot{Q}} = \frac{Q}{t_{sol}}, \tag{2}$$

where the thermal energy referring to the solidification of the cell is Q and the solidification time is t_{sol}, which is set to t_{sol}^{init} to calculate $\overline{\dot{Q}}$ for the first cell. The mean HTF outlet temperature during the solidification of any cell is determined by Eq. (3):

$$\overline{T_{out}} = \overline{T_{in}} + \frac{\overline{\dot{Q}}}{\dot{m} \bullet c_p} \tag{3}$$

where the HTF mass flow is $\dot{m}$ and its heat capacity c_p, while the HTF inlet mean temperature is $\overline{T_{in}}$, which is T_{in}^{LTES} for the first cell. Now, it is possible to calculate s_{next} – the distance that is solidified when the previous cell has completed solidification – for the next cell (Eq. (4)):

$$s_{next} = \sqrt{2 \bullet \frac{\lambda \bullet \left(T_m - \overline{T_{out}^{i-1}}\right)}{L \bullet \rho} \bullet t_{sol}^{i-1}}, \tag{4}$$

where $\overline{T_{out}^{i-1}}$ and t_{sol}^{i-1} refer to the previous cell. The complete solidification time for the cell under consideration is given by Eq. (5):

$$t_{sol} = t_{sol}^{i-1} + \frac{s^2 - s_{next}^2}{s^2} \bullet t_{sol}^{init} \tag{5}$$

This procedure can be repeated until the last cell is reached, which gives the solidification time of the overall LHTESS. However, since $\frac{s_{next}}{s}$ was found to be identical for all cells, the solidification time of the overall LHTESS t_{sol}^{LTES} can be calculated simply with Eq. (6) (a detailed derivation can be found in Appendix A):

Table 4
List of the different variants of the UA approach used in this work.

Identifiers	Description
UA approach 1a	The heat transfer resistance in the HTF is neglected and the UA approach is used to predict the discharging time (t_{sol}^{LTES}) without the help of a reference solution.
UA approach 2a	The heat transfer resistance in the HTF is taken into account and the UA approach is used to predict t_{sol}^{LTES} without the help of a reference solution.
UA approach 1b	The heat transfer resistance in the HTF is neglected and a UA value is estimated from a reference solution and t_{sol}^{LTES} is predicted with the help of this UA value.
UA approach 2b	The heat transfer resistance in the HTF is taken into account and a UA value is estimated from a reference solution and t_{sol}^{LTES} is predicted with the help of this UA value.

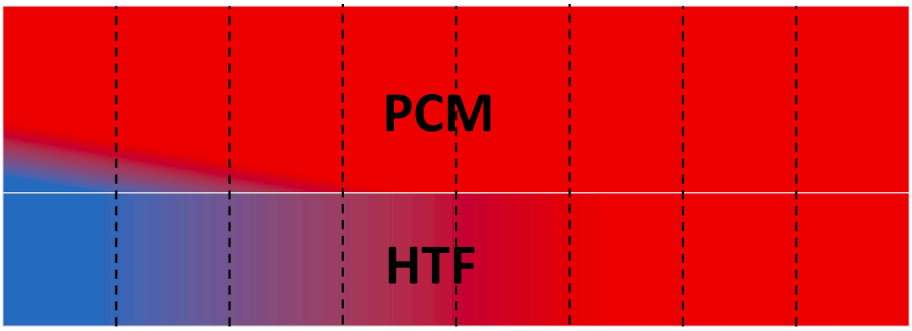

Fig. 2. Discretization of the domain considered for the development of the UA approach.

$$t_{sol}^{LTES} = \left(1 + \frac{UA}{\dot{m} \bullet c_p}\right) \bullet \frac{Q_{LTES}}{UA \bullet \left(T_m - T_{in}^{LTES}\right)}, \tag{6}$$

where Q_{LTES} is the thermal energy of the whole LHTESS and UA is defined by Eq. (7):

$$UA = 2 \bullet \frac{A \bullet \lambda}{s} \tag{7}$$

where the heat transfer area is A and the thermal conductivity of the PCM is λ. By inserting the NTU in Eq. (6), it can be reformulated to Eq. (8):

$$t_{sol}^{LTES} = (1 + NTU) \bullet t_{sol}^{init} \tag{8}$$

3.2. Included heat transfer resistance in the HTF towards the PCM (UA approach 2a)

The case is similar to the UA approach 1a; however, in this case, the heat transfer resistance within the HTF towards the PCM is taken into account. Accordingly, the initial solidification time t_{sol}^{init} can be calculated with Eq. (9) [12]:

$$t_{sol}^{init} = \left(\frac{s}{2 \bullet \lambda} + \frac{1}{k}\right) \bullet L \bullet \rho \bullet s \bullet \frac{1}{T_m - T_{in}^{LTES}} \tag{9}$$

The heat transfer coefficient k equals the convective heat transfer coefficient here, but can also be adjusted to account for the resistance of a pipe or container wall. Eq. (10) allows s_{next} to be calculated:

$$s_{next} = \frac{\lambda \bullet \left(\sqrt{\frac{2 \bullet t_{sol}^{i-1} \bullet \left(T_m - \overline{T_{out}^{i-1}}\right) \bullet k^2}{L \bullet \rho \bullet \lambda}} + 1 - 1\right)}{k} \tag{10}$$

and Eq. (11) allows t_{sol} to be determined:

$$t_{sol} = t_{sol}^{i-1} + \frac{Q}{\left(UA \bullet \left(T_m - T_{in}^{LTES}\right)\right)} - \frac{Q_{s_{next}}}{\left(UA_{s_{next}} \bullet \left(T_m - T_{in}^{LTES}\right)\right)}, \tag{11}$$

where $Q_{s_{next}}$ is the heat referring to the solidification front at the position s_{next}. Eq. (12) defines the UA value of one cell UA:

$$UA^{cell} = 2 \bullet \frac{A}{\left(\frac{s}{\lambda} + \frac{2}{k}\right) \bullet n_{cells}} \tag{12}$$

where n_{cells} is the number of cells and UA_{next}^{cell} can be determined with Eq. (13):

$$UA_{next}^{cell} = 2 \bullet \frac{A}{\left(\frac{s_{next}}{\lambda} + \frac{2}{k}\right) \bullet n_{cells}} \tag{13}$$

Since it was observed that $\frac{s_{next}}{s}$ also remains constant in this approach, the solidification time of the whole LHTESS can be calculated with Eq. (14):

$$t_{sol}^{LTES} = \left(Q \Big/ \left(UA^{cell} \bullet \left(T_m - \overline{T_{in}^{i=2}}\right)\right) - Q_{s_2} \Big/ \left(UA_{s_2}^{cell} \bullet \left(T_m - \overline{T_{in}^{i=2}}\right)\right)\right) \bullet n_{cells} + t_{init} \tag{14}$$

where Q_{s_2}, $UA_{s_2}^{cell}$ and $\overline{T_{in}^{i=2}}$ refer to the second cell. It was found that the result does not depend on n_{cells} and it can therefore be set to 1, thus simplifying Eqs. (12)–(14). The procedure for calculating the solidification time of the overall LHTESS is as follows:

- Calculate UA with Eq. (12)
- Calculate t_{sol}^{init} with Eq. (9)
- Calculate $\dot{Q}$ and $\overline{T_{out}}$ with Eqs. (2) and (3)
- Calculate s_{next} with Eq. (10)
- Calculate UA_{next}^{cell} with Eq. (13)
- Calculate t_{sol}^{LTES} with Eq. (14)

3.3. Determine the UA value by means of a reference solution (UA approach 1b and UA approach 2b)

In the methods above described, the solidification time of the LHTESS was estimated using the properties of the materials, the geometry of the LHTESS and the initial and boundary conditions. In this section, a different approach is embraced. Here, the results of an experiment or a detailed simulation are employed to calculate a UA value of the LHTESS, which is subsequently used to estimate the performance of the LHTESS for different initial and boundary conditions, as well as for other dimensions or material properties. For the case of negligible heat transfer resistance in the HTF (approach 1b), the UA value can be calculated by rearranging Eq. (6), which leads to Eq. (15):

$$UA = \frac{Q}{t_{sol}^{LTES} \bullet \left(T_m - T_{in}\right) - \frac{Q}{\dot{m} \bullet c_p}} \tag{15}$$

To estimate t_{sol}^{LTES} for different conditions, the UA value is inserted into Eq. (6). If the thermal conductivity or the dimensions are varied, the UA value has to be adjusted in a linear manner, following Eq. (7).

If the heat transfer resistance cannot be neglected, the UA value cannot be determined a priori and more information, such as k or $\frac{s}{\lambda}$, has to be available. For instance, when k is known, the overall UA value can be estimated with the help of a simple optimization (e.g.: an approach similar to the downhill simplex method [32]) by calculating an estimated t_{sol}^{LTES} with a guess for $\frac{s}{\lambda}$ and comparing it to the actual t_{sol}^{LTES}. In this case, the optimization criterion would be to minimize the difference between the estimated and the real t_{sol}^{LTES} by adjusting $\frac{s}{\lambda}$. The procedure for the UA approaches 1b and 2b for calculating the solidification time of the LHTESS is as follows:

- Get t_{sol}^{LTES} for one case from an experiment or a simulation
- For UA approach 1b, determine the UA value with Eq. (15)
- For UA approach 2b, calculate the UA value, whereby k or $\frac{s}{\lambda}$ has to be known and the other can be guessed. Adjust the guess by comparing the t_{sol}^{LTES} resulting from the calculated UA value with the measured or simulated t_{sol}^{LTES}.
- For UA approaches 1b and 2b use the determined UA value for one of the following two options:
  - Calculate t_{sol}^{LTES} for different boundary conditions.
  - Calculate t_{sol}^{LTES} for a variation in the UA value – for instance, for the UA approach 1b, an increase in the thermal conductivity by 100 % also increases the UA value by 100 % (see Eq. (7)).

4. Results and discussion

This section is divided into two parts. First, the results based on predicting the discharging time from solely the material properties, the geometry and the boundary and initial conditions are shown and discussed (UA approaches, 1a and 2a). Second, those results that deal with approaches 1b and 2b are presented.

4.1. Results of the UA approaches 1a and 2a

This section examines the degree to which the results of the UA approach (1a and 2a) agree with those of the reference solution and the factors that influence the said agreement. To do so, the results are compared to those of the reference solution for different Ste, Bi, HTF and $\dot{m}$. Throughout this section, the UA results refer to approach 1a (neglecting the thermal resistance in the HTF), unless otherwise indicated. Similarly, air was used as the HTF, unless explicitly indicated. For the UA approach, three different results are shown in each figure throughout the section; these refer to different amounts of energy being

taken into account. A definition of the three cases can be found in Table 5. The first case (L_{lat}) only takes the latent heat into account, while the last case ($L_{lat,sen\ B}$) includes all of the sensible heat. The case in the middle ($L_{lat,sen\ A}$) takes into account the sensible heat that corresponds to a complete solidification with an infinite mass flow (no temperature change of the HTF throughout the LHTESS).

In Fig. 3, the results for the discharging time are shown over the HTF mass flow rate ($\dot{m}$) for the following conditions: $L = 200\mathrm{kJ/kg}$, $c = 200\mathrm{J/(kgK)}$, $\lambda = 0.1\mathrm{W/(mK)}$ and $k = 1000\mathrm{W/(m^2K)}$; which results in $Ste = 0.02$ and $Bi = 500$. The UA approach is compared with the results obtained with the detailed numerical model. In Fig. 4, the discharging time results are provided for the same conditions, but with $\lambda = 2\mathrm{W/(mK)}$; resulting in $Bi = 25$.

In both cases, it can be noted that the discharging time of the reference solution depends strongly on the stopping criterion Q_{Stop}, i.e.: the relative amount of energy that has to be released in order to consider that the LHTESS has completed its discharge. For instance, $Q_{Stop} = 99.9\%$ refers to 99.9 % of the theoretical maximum of the energy that can be discharged. The slope of the results of the UA approach is very similar to that of the reference solution and, in general, the absolute values fit the one referring to $Q_{Stop} = 99.9\%$. The fit only shifts to a lower Q_{Stop} for high mass flows and $\lambda = 2\mathrm{W/(mK)}$. Finally, as expected, the difference between the different definitions of L_{eff} is small. The relative deviation of the UA approach from the reference solution is shown in Table C 1 in the Appendix. The mean error $\bar{\varepsilon}$ is always below 5 % for $Q_{Stop} = 99.9\%$ and $Q_{Stop} = 99\%$. The relative variation of the reference solution Δt_{ref} is also shown in Table C 1 and helps to better judge $\bar{\varepsilon}$. For the case shown in Fig. 3, Δt_{ref} is about 10 % and, for the case shown in Fig. 4, it is more than 70 %.

The results presented in Fig. 5 explore whether the UA approach can simulate LHTESS systems that include an amount of HTF that represents a large storage capacity (in addition to the PCM), which is a typical situation in many actual systems. This situation especially affects the beginning of the discharge process. For this purpose, water was used as a HTF and the HTF volume was increased to 1 $\mathrm{m^3}$. It was assumed that the HTF is pushed out following a plug flow and the time taken to do so was simply added to the discharging time. This led to a picture similar to the cases shown in Figs. 3 and 4: the slope of the UA approach fits the reference solutions to a large extent and the absolute values refer to high Q_{Stop}. If the time needed to push the HTF out is not taken into account, the UA approach diverges strongly from the reference solution, especially for small mass flow rates. The relative deviations of the UA approach from the reference solution are shown in Table C 1 in the Appendix. If the HTF is taken into account, $\bar{\varepsilon}$ can be as low as 2–3 %; while $\bar{\varepsilon}$ is always larger than 30 % if the HTF is not included.

Next, in Fig. 6, we assess a case where the heat transfer resistance in the HTF cannot be neglected. The case is for most parameters identical to the one shown in Fig. 4 ($L = 200\mathrm{kJ/kg}$, $c = 200\mathrm{J/(kgK)}$ and $\lambda = 2\mathrm{W/(mK)}$), but k was set to $100\mathrm{W/(m^2K)}$, resulting in $Bi = 2.5$. Fig. 6 shows that, if the heat transfer resistance in the HTF is included in the UA approach, its results almost perfectly fit the one for Q_{Stop} 99.9% of the reference solution – $\bar{\varepsilon}$ is 0.7 to 1.6 % (see Table C 1 in the Appendix). If this resistance is not taken into account, the results of the UA approach are far from the reference solution, leading to a $\bar{\varepsilon}$ of about 20 to 35 % over all the Q_{Stop}.

Setting $c = 2000\mathrm{J/(kgK)}$, which results in a more realistic Ste of 0.2, gave results that still follow the slope of the reference solution to a large extent, but the deviation between the UA approach and the reference solution is now larger (see Figs. 7 and 8 and Table C 1 in the Appendix). The difference between the definitions of L_{eff} is also significant for this case, leading to a $\bar{\varepsilon}$ that varies by about 10 to 20 %-points for different L_{eff}. The above findings are even more pronounced if the Ste is further increased to a sensible storage (Figs. B1 and B2 and Table C 1 in the Appendix). It can be noted that the absolute values of t_{sol}^{LTES}, obtained with the UA approach, coincide with lower Q_{Stop} of the reference solution when the Ste is increased. This behavior can be explained by the increased amount of sensible heat due to the larger Ste – as a direct consequence, there is also an increase in the sensible heat still in the LHTESS when solidification is completed.

Table 5
Definitions of different energies taken into account in the UA approaches.

Identifier	Short form	Energy taken into account
UA approach latent energy	L_{lat}	$L_{eff} = L$
UA approach latent + sensible energy A	$L_{lat,sen\ A}$	$L_{eff} = L + [0.5 \bullet (T_m - T_{in}) + (T_{init} - T_m)] \bullet c$
UA approach latent + sensible energy B	$L_{lat,sen\ B}$	$L_{eff} = L + (T_{init} - T_{in}) \bullet c$

5. Discussion

For all the cases studied so far, the results of the UA approach follow, to a large extent, the slope of the reference solution for t_{sol}^{LTES} over $\dot{m}$. Moreover, the UA approach can account for a heat transfer resistance between the HTF and the PCM and, in addition, different HTF, including large capacities initially in the LHTESS. However, the absolute values achieved for t_{sol}^{LTES} mimic different Q_{Stop} of the reference solution. Looking at the range from Q_{Stop} 90 % to Q_{Stop} 99.9 %, this can lead to errors of more than 30 % in t_{sol}^{LTES}; the higher the Ste, the more severe this problem is. In conclusion, the UA approach 1a and 2a can be used for a preliminary estimation of the discharging time of the LHTESS, especially for small Ste, and it can help to understand the influence of different input parameters. In the following section, we analyze whether the use of a reference value obtained by numerical simulations or experiments leads to an improvement in the prediction accuracy.

5.1. Results of the UA approaches 1b and 2b

In this section, the results of the UA approaches 1b and 2b are presented. In both cases, the results achieved with the numerical model are used to estimate a UA value (and further properties in the case of the UA approach 2b), which is then used to predict t_{sol}^{LTES} for different conditions.

5.1.1. Results of the UA approach 1b

In the following, the results using the UA approach 1b are shown and discussed. Two different cases are studied. In the first, a UA value is estimated from the numerical results with Eq. (15); this UA value is then used in Eq. (6) to predict t_{sol}^{LTES} for different $\dot{m}$. In the second case, Eq. (15) is again applied to estimate a UA value. This UA value is then adjusted for a variation of λ with Eq. (7), and finally Eq. (6) is used to predict t_{sol}^{LTES}.

For both cases, the material properties were set to $L = 200\mathrm{kJ/kg}$, $c = 2000\mathrm{J/(kgK)}$ and $k = 1000\mathrm{W/(m^2K)}$, which results in $Ste = 0.2$; whereas λ and $\dot{m}$ were varied. In the first case, Q_{Stop} was set to 90 %, 99 % or 99.9 % and the effective melting enthalpy was always set according to the "UA approach latent + sensible energy B".

Next, the discharging time is plotted over $\dot{m}$ for the reference solution and the results achieved with the UA approach. The results shown in Fig. 9, Figs. B3 and B4 in the Appendix correspond to $\lambda = 0.1\mathrm{W/(mK)}$; the results in Figs. B5 to B7 in the Appendix correspond to $\lambda = 0.5\mathrm{W/(mK)}$; and the results in Fig. 10 and Figs. B8 and B9 in the Appendix correspond to $\lambda = 2\mathrm{W/(mK)}$. In addition to λ, the mass flow present while estimating the UA value was also varied. For the results in Figs. B3, B5 and B8 in the Appendix, it was set to $\dot{m} = 0.1\ \mathrm{kg/s}$; for those in Figs. 9 and 10 and Fig. B6 in the Appendix, it was set to $\dot{m} = 0.7743\ \mathrm{kg/s}$; while for those in Figs. B4, B7 and B9 in the Appendix, it was set to $\dot{m} = 10\ \mathrm{kg/s}$. In Table C 2 in the Appendix, all the $\bar{\varepsilon}$ are also listed together with Δt_{ref}.

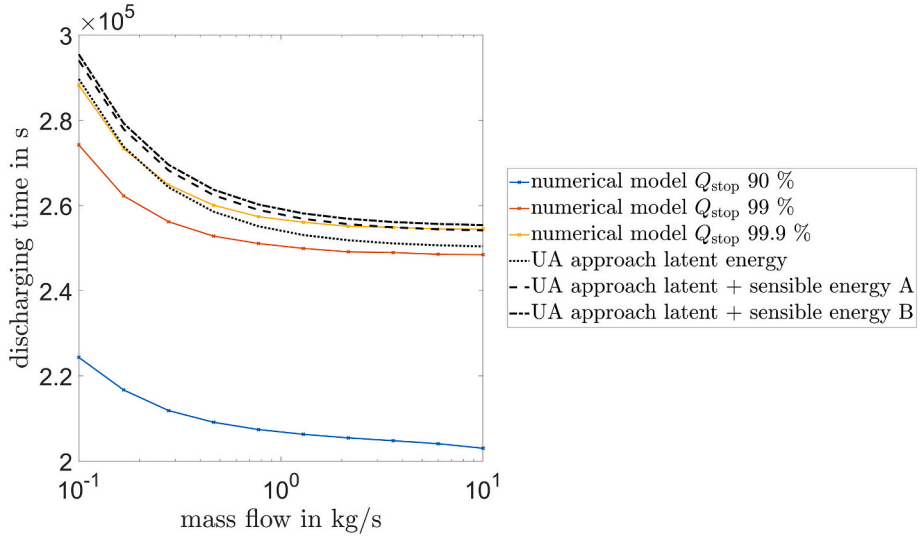

Fig. 3. Reference solution and predicted discharging times for the UA approach 1a for $\lambda = 0.1\mathrm{W/(mK)}$, $c = 200\mathrm{J/(kgK)}$, $k = 1000\mathrm{W/(m^2K)}$ and $L = 200000\mathrm{J/kg}$ (yields $Ste = 0.02$ and $Bi = 500$).

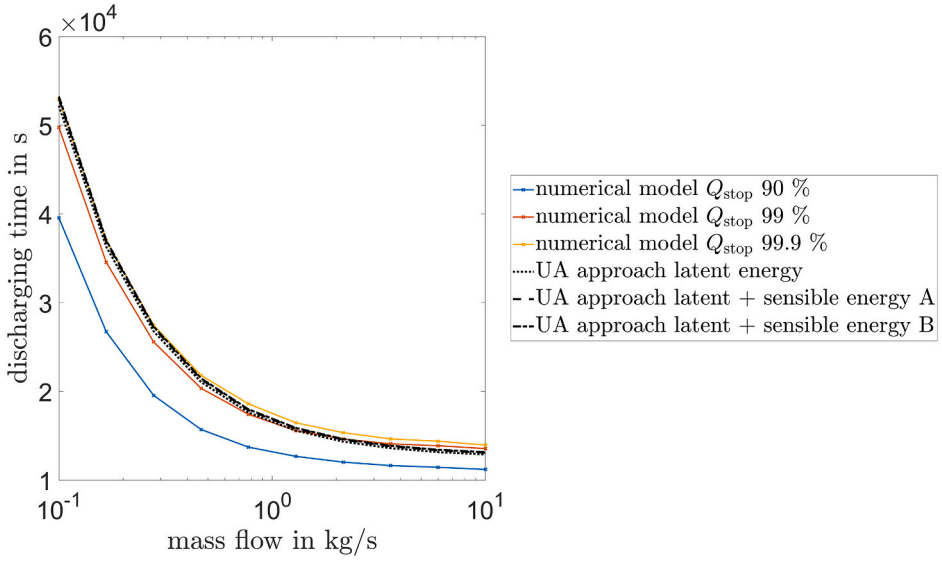

Fig. 4. Reference solution and predicted discharging times for the UA approach 1a for $\lambda = 2.0\mathrm{W/(mK)}$, $c = 200\mathrm{J/(kgK)}$, $k = 1000\mathrm{W/(m^2K)}$ and $L = 200000\mathrm{J/kg}$ (yields $Ste = 0.02$ and $Bi = 25$).

As expected, for the $\dot{m}$ used to estimate the UA values, the results of the UA approach are identical to those of the reference solution. If $\dot{m}$ is increased, t_{sol}^{LTES} is predicted too small; while if $\dot{m}$ is decreased, t_{sol}^{LTES} is predicted too large. Analyzing the $\overline{\varepsilon}$ for all the cases shown in Table C 2 reveals that the smallest deviations resulted when the mass flow was set to $\dot{m} = 0.7743\ \mathrm{kg/s}$ for estimating the UA value (somewhere in the middle of the parameter space). Setting $\dot{m}$ to the highest ($10\ \mathrm{kg/s}$) or lowest ($0.1\ \mathrm{kg/s}$) values give identical maximum deviations, but the average over the mass flow range is lower when the mass flow was set to $\dot{m} = 10\ \mathrm{kg/s}$. For $\lambda = 0.1\mathrm{W/(mK)}$, $\overline{\varepsilon}$ is always below 10 %, but for $\lambda = 2\mathrm{W/(mK)}$, the deviation of a single calculation can reach more than 100 %, resulting in negative t_{sol}^{LTES} for $\lambda = 2\mathrm{W/(mK)}$ (Fig. B8 in the Appendix). Furthermore, Q_{Stop} has a large influence on the deviations, while larger Q_{Stop} values lead to smaller deviations (see Table C 2 in the Appendix). For $Q_{Stop} = 99.9\%$, the maximum of $\overline{\varepsilon}$ is 12.9 %, and for most cases it is below 5 %. When it comes to the influence of λ, it can be seen that an increase in λ leads to an increase in $\overline{\varepsilon}$ and Δt_{ref}.

Even though there were large $\overline{\varepsilon}$ in some cases, it should be kept in mind that the variation of $\dot{m}$ was performed over two orders of magnitude. Generally speaking, a reasonable prediction of t_{sol}^{LTES} can be achieved for $\dot{m}$ up to an order of magnitude larger or smaller than the value used for predicting the UA value.

The UA approach 1b was also applied to predict t_{sol}^{LTES} for the same case as in the reference solution, but with a different λ value. In Fig. 11, the results are shown for using $\lambda = 0.1\mathrm{W/(mK)}$ in the reference case and predicting t_{sol}^{LTES} for higher λ values. In Fig. 12, the results are presented for using $\lambda = 2\mathrm{W/(mK)}$ in the reference solution and predicting t_{sol}^{LTES} for lower λ values. In both cases, this was performed for a variety of Q_{Stop} and $\dot{m}$ value combinations. The values for $\overline{\varepsilon}$ are shown in Table C 3 in the Appendix. Predicting t_{sol}^{LTES} for higher λ values based on the results referring to $\lambda = 0.1\mathrm{W/(mK)}$ works remarkably well. A $\overline{\varepsilon}$ of more than 7 % can only be observed for the variation with $\dot{m} = 0.1\ \mathrm{kg/s}$ and Q_{Stop} 90%. In the other case – predicting t_{sol}^{LTES} from a reference solution using $\lambda = 2\mathrm{W/(mK)}$ for lower λ values – the outcome is different. For

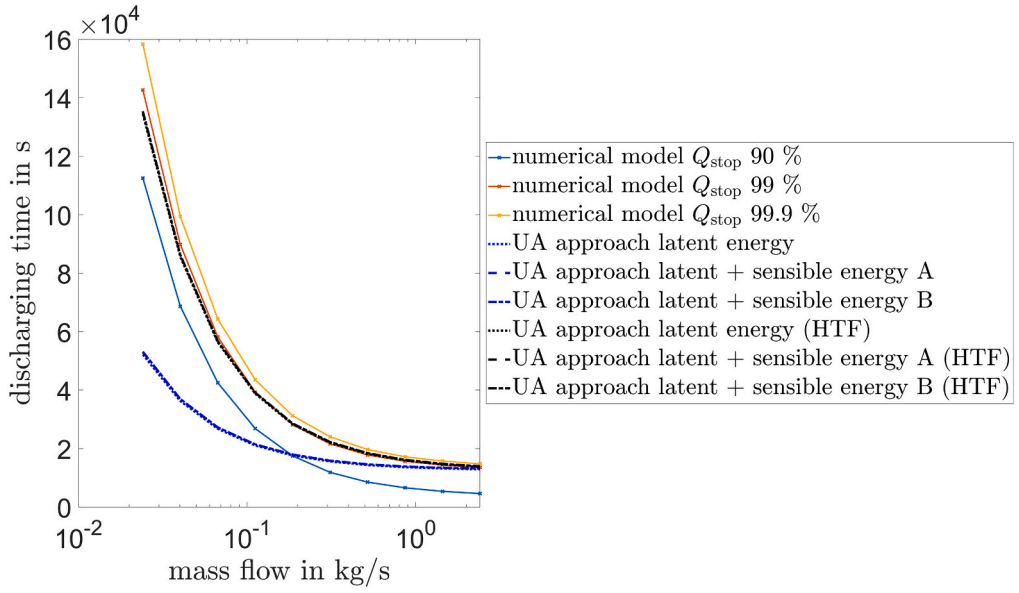

Fig. 5. Reference solution and predicted discharging times for the UA approach 1a for $\lambda = 2.0\mathrm{W/(mK)}$, $c = 200\mathrm{J/(kgK)}$, $k = 1000\mathrm{W/(m^2K)}$ and $L = 200000\mathrm{J/kg}$ with water as heat transfer fluid (HTF) and $V_{HTF} = 1m^3$(yields $Ste = 0.02$ and $Bi = 25$).

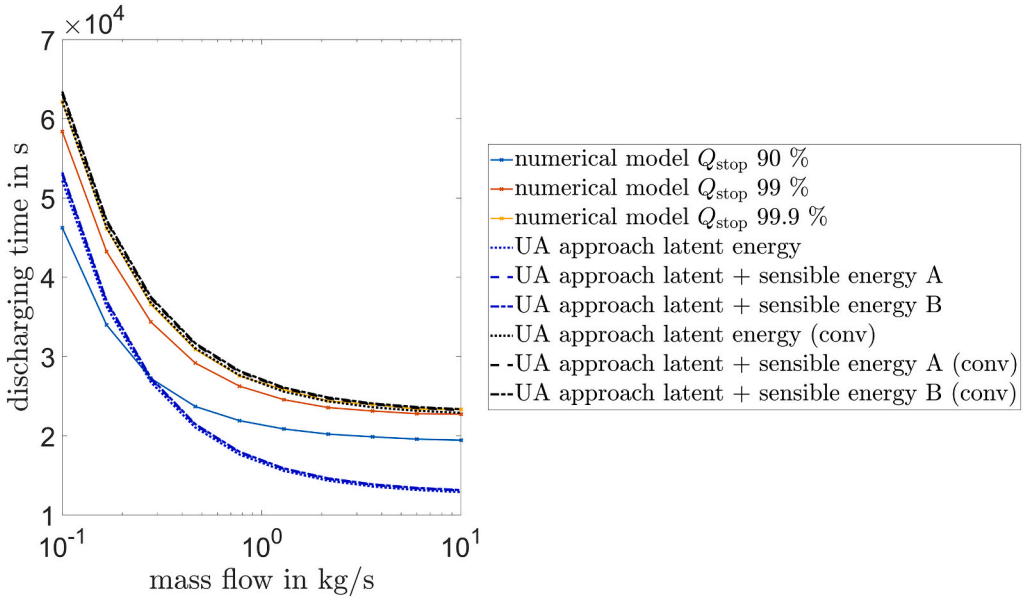

Fig. 6. Reference solution and predicted discharging times for the UA approach 2a for $\lambda = 2.0\mathrm{W/(mK)}$, $c = 200\mathrm{J/(kgK)}$, $k = 100\mathrm{W/(m^2K)}$ and $L = 200000\mathrm{J/kg}$ (yields $Ste = 0.02$ and $Bi = 2.5$) – once neglecting the thermal resistance from the heat transfer fluid to the pipe and once taking it into account (indicated by (conv)).

most cases, $\overline{\varepsilon}$ is now twice as high, and for the case with Q_{Stop} 90 % and $\dot{m} = 0.1$ kg/s, it reaches almost 65 %. Moreover, it is worth noting that, for both cases, it holds that the larger the difference between the lambda of the reference solution and the lambda of the predicted value, the higher the deviation for t_{sol}^{LTES}. Interestingly, the deviation is positive in some cases and negative for others.

5.1.2. Results of the UA approach 2b

In this section, the same procedure as in the section before is followed, but with the UA approach including the heat transfer resistance between PCM and HTF. In Figs. B10 to B18 in the Appendix, the prediction for different $\dot{m}$ can be seen. Due to the additional heat transfer resistance, the discharging times are all longer than for the UA approach 1b. When it comes to the difference between the reference solution and the predictions, the results are fairly identical to those of the UA approach 1b (see Table C 2 in the Appendix).

The prediction for different λ worked – as for the UA approach 1b – very well for a prediction for higher λ values based on the results for $\lambda = 0.1\mathrm{W/(mK)}$ (see Fig. B19 and Table C 3 in the Appendix). Furthermore, the prediction for lower λ values led to higher deviations between reference and prediction, similar to the UA approach 1b, but the deviations differ and, in some cases, have different signs (compare Fig. 12 and Fig. B20 in the Appendix).

5.1.3. Discussion on UA approach 1b and UA approach 2b

Predicting the discharging time of an LHTESS based on a reference solution works for UA approaches 1b and 2b. The reference solution can be a numerical simulation – as it is here – or experimental results.

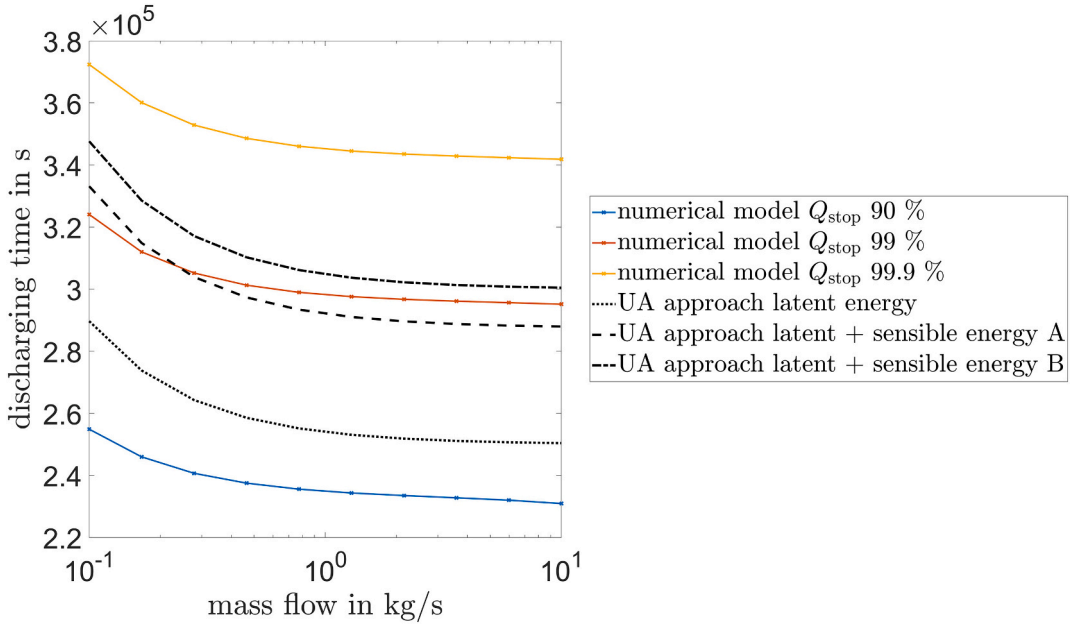

Fig. 7. Reference solution and predicted discharging times for the UA approach 1a for $\lambda = 0.1\mathrm{W/(mK)}$, $c = 2000\mathrm{J/(kgK)}$, $k = 1000\mathrm{W/(m^2K)}$ and $L = 200000\mathrm{J/kg}$ (yields $Ste = 0.2$ and $Bi = 500$).

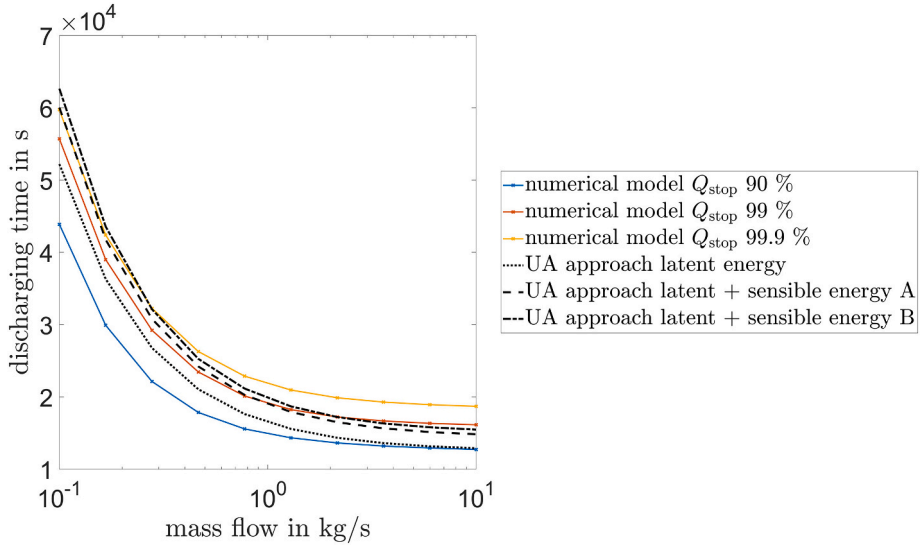

Fig. 8. Reference solution and predicted discharging times for the UA approach 1a for $\lambda = 2.0\mathrm{W/(mK)}$, $c = 2000\mathrm{J/(kgK)}$, $k = 1000\mathrm{W/(m^2K)}$ and $L = 200000\mathrm{J/kg}$ (yields $Ste = 0.2$ and $Bi = 25$).

Interestingly, the quality of the prediction was almost identical for most cases for the UA approaches 1b and 2b. The prediction works somewhat better when the performance of an LHTESS with a different λ of the PCM is studied compared to the prediction of the performance under different $\dot{m}$ of the HTF. The smallest deviations between the prediction and reference solution were seen for both UA approaches for an LHTESS with a PCM and $\lambda = 0.1\mathrm{W/(mK)}$, whose performance was predicted for higher λ values.

The reason for this behavior can be explained by looking at how errors in the UA calculation propagate throughout the prediction process. For low λ values, the NTU is small and t_{sol}^{LTES} is close to t_{sol}^{init} (see Eq. (8)). Consequently, an error in e.g., t_{sol}^{LTES} by 1% can be compensated by a change of UA of about -1%. In contrast, a much stronger adjustment must be made for higher λ values. This leads to the prediction of the UA value being more accurate for small λ values. When predicting the discharging time for other λ values, this effect is amplified by the fact that an error in the UA prediction has a smaller influence on t_{sol}^{LTES} for high λ values than for small λ values (see Eq. (8)). In short, for small λ values, the determination of the UA value is more accurate and an error in the UA value has a smaller influence on the prediction of t_{sol}^{LTES} (towards higher λ values) than for high λ values. In case the reference solution can be freely chosen, we therefore recommend to select it in such a way that the thermal conductivity of the PCM is at the lower end and the HTF mass flow is in the middle of that of the parameter field.

5.1.4. Comparison to recent approaches

Compared to the work of Raud et al. [26] we included the convective heat transfer resistance between HTF and PCM, added sensible heat in a simplified form, successfully tested the incorporation of reference solutions to increase the accuracy and varied the boundary conditions to a

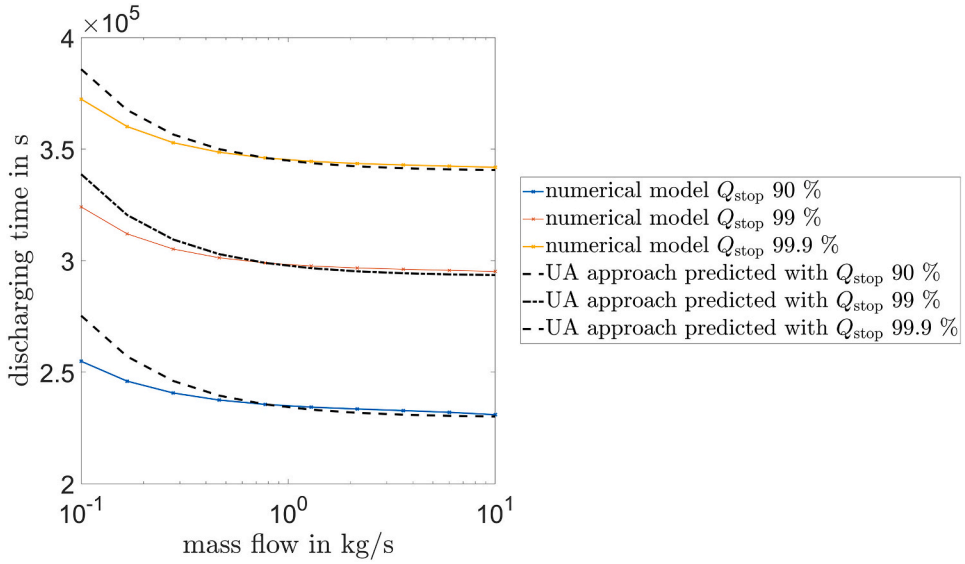

Fig. 9. Reference solution and predicted discharging times based on results with $\dot{m} = 0.7743 kg/s$ for the UA approach 1b for $\lambda = 0.1\mathrm{W/(mK)}$, $c = 2000\mathrm{J/(kgK)}$, $k = 1000\mathrm{W/(m^2K)}$ and $L = 200000\mathrm{J/kg}$ (yields $Ste = 0.2$ and $Bi = 500$).

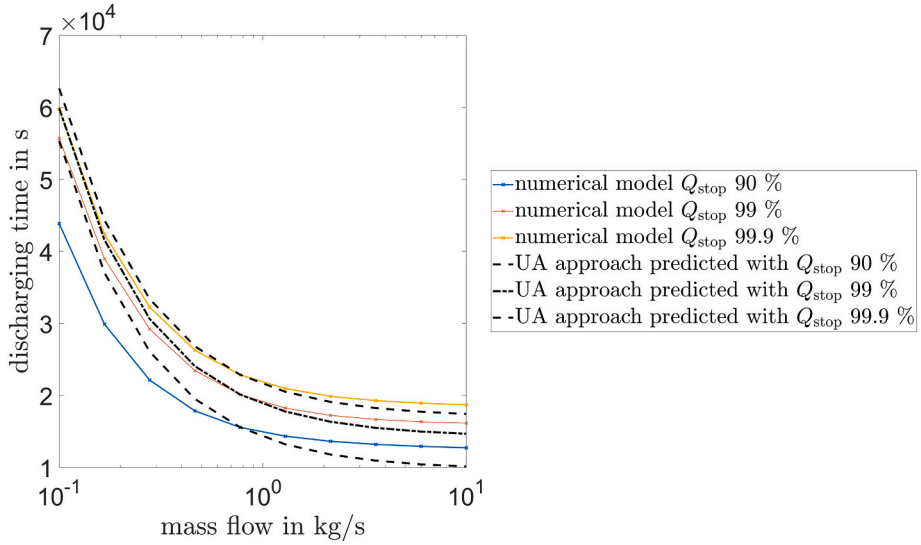

Fig. 10. Reference solution and predicted discharging times based on results with $\dot{m} = 0.7743 kg/s$ for the UA approach 1b for $\lambda = 2.0\mathrm{W/(mK)}$, $c = 2000\mathrm{J/(kgK)}$, $k = 1000\mathrm{W/(m^2K)}$ and $L = 200000\mathrm{J/kg}$ (yields $Ste = 0.2$ and $Bi = 25$).

large extend to check the validity of the approach. Raud et al. [26] on the other hand included finned heat exchangers in their approach and performed a cost analysis of the LHTESS.

An overview of the similarities and differences of the UA approach compared to the work of Beyne et al. [28] is shown in Table 6.

6. Summary

A method for analytically calculating the discharging time of an LHTESS in plate design was developed and tested. The basis of the method is similar to one already presented in the literature for an LHTESS with macro-encapsulated PCM [12]. Both approaches assume quasi-stationary conditions, neglect the sensible heat in the heat transfer process and add it later to an L_{eff}. Furthermore, the idea of using temporal mean values for the inlet temperature for each cell of the LHTESS (to derive the method the storage is divided into a certain number of cells – similar to the discretization process for numerical simulation), for instance, is common in both approaches. The differences to two recent and also similar approaches [26,28] were discussed in detail as well.

We show that our approach – here called the UA approach – can be formulated independently of the number of cells, leading to simple equations for calculating the discharging time. In the case of large Bi (the heat transfer resistance between the HTF and PCM is neglected), it can be determined with the help of the NTU and an initial discharging time (see Eq. (8)). The initial discharging time equals the quasi-stationary solidification time of the very first part of the LHTESS – or, in other words, the solidification time with the inlet condition of the HTF as a boundary condition.

The UA approach was then tested for a broad range of boundary conditions and compared to the results of a validated numerical model. The results are promising, but the deviations reported here are on average higher than those reported in the literature [12]. As expected, the results of the UA approach mimic the reference solution to a large extent for small Ste, also for Ste $= 0.2$, or even for sensible thermal

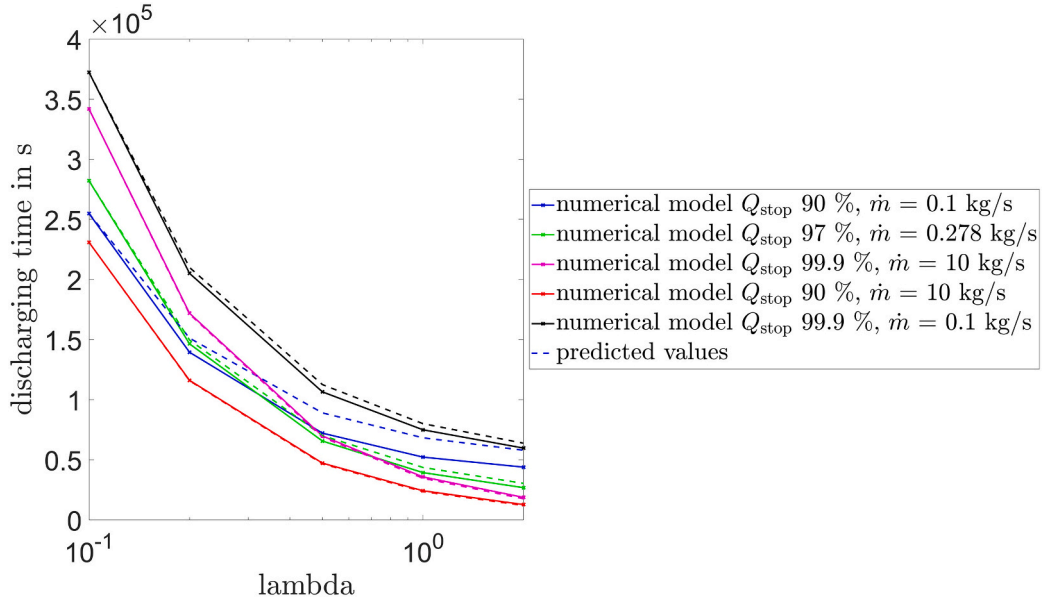

Fig. 11. Reference solution and predicted discharging times based on results with $\lambda = 0.1\text{W}/(\text{mK})$ for the UA approach 1b for $c = 2000\text{J}/(\text{kgK})$, $k = 1000\text{W}/(\text{m}^2\text{K})$ and $L = 200000\text{J}/\text{kg}$ (yields $Ste = 0.2$).

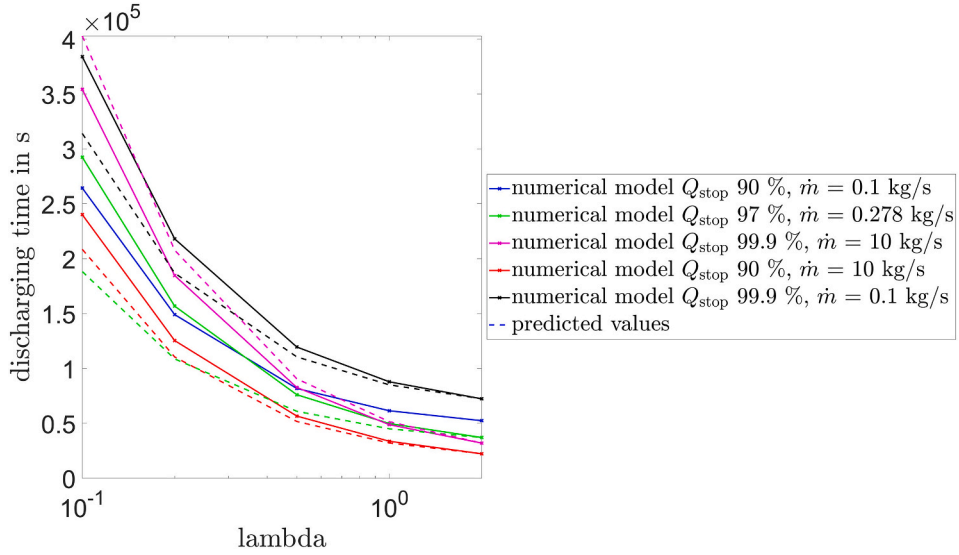

Fig. 12. Reference solution and predicted discharging times based on results with $\lambda = 2.0\text{W}/(\text{mK})$ for the UA approach 1b for $c = 2000\text{J}/(\text{kgK})$, $k = 1000\text{W}/(\text{m}^2\text{K})$ and $L = 200000\text{J}/\text{kg}$ (yields $Ste = 0.2$).

Table 6
Comparison of the UA approach with the method presented by Beyne et al. [28].

	UA approach	Beyne et al. [28]
Geometry	Only plate design	Different designs
Sensible heat	Included in a simplified way	Neglected
Thermal energy of HTF	Included in a simplified way	Neglected
Time dependency	Mean values	Time series
Complexity of approach	Low to medium	Somewhat higher than the UA approach
Tests	Tested over a broad range of parameters	Tested for the same assumptions underlying the derivation
Incorporation of reference solutions	Successfully tested	Not tested

energy storage, the slope of the results over $\dot{m}$ is similar, but the absolute values may refer to different Q_{stop} of the reference solution.

Finally, we checked if it is possible to take one reference solution and predict the behavior under different $\dot{m}$ of the HTF, or higher or lower λ values of the PCM. This test is of particular practical interest since, if successful, it would allow results from numerical simulations or even experiments to be used to predict the behavior under different conditions. Moreover, not all physical parameters have to be known to apply this procedure, enabling some kind of black box treatment of an experiment. The results reveal that, for the parameters tested, predicting the discharge time for higher lambda values works remarkably well (here the reference solution had $\lambda = 0.1\text{W}/(\text{mK})$ and the predictions were performed until $\lambda = 2.0\text{W}/(\text{mK})$). Furthermore, testing the other way around – predicting the discharging time for lower λ values – and predicting the discharging time for different $\dot{m}$ of the HTF gave promising results, as long as the variation is not too large. The reason why the

prediction of the discharging time works better from low to high λ values is that, for small λ values, the determination of the UA value is more accurate and an error in the UA value has a smaller influence on the prediction of t_{sol}^{LTES} (towards higher λ values) than for high λ values.

There are myriad ways in which the UA approach can be used and further developed in the future. Some of these are to:

- Check how the UA approach performs with experiments instead of numerical results.
- Apply the UA approach to other geometries.
- Predict not only the discharging time, but also the outlet temperature.
- Deepen the understanding of how physical parameters, as well as initial and boundary conditions, affect the performance of the UA approach.
- Investigate whether the approach can also be applied to melting processes.
- Check if one can calculate t_{sol}^{init} in Eq. (8) in a different way, e.g., by numerical simulations or correlations for more complex geometries.
- Combine the UA approach with a recently presented alternative analytical method to describe the discharging of LHTESS [28]

Nomenclature

Variables and abbreviations

A	area in m^2
Bi	Biot number
c	specific heat capacity in $J/(kgK)$
c_p	specific heat capacity of the HTF in $J/(kgK)$
h	height in m
HTF	heat transfer fluid
k	heat transfer coefficient in $W/(m^2K)$
l	length in m
L	melting enthalpy in J/kg
LHTESS	latent heat thermal energy storage systems
$\dot{m}$	mass flow in kg/s
n	count variable
NTU	number of transfer units
Q	heat in J
$\dot{Q}$	thermal power in W
PCM	phase change material
s	thickness in m
Ste	Stefan number
t	time in s
T	temperature in K
UA	heat transfer coefficient times the area in W/K
V	volume in m^3
Δt	relative time difference
$\overline{\varepsilon}$	mean error
λ	thermal conductivity in $W/(mK)$
ρ	density in kg/m^3

Subscripts

$_{cells}$	cells
$_{eff}$	effective
$_{HTF}$	heat transfer fluid
$_{in}$	inlet condition
$_{init}$	initial condition
$_{lat}$	latent heat
$_{lat,sen\ A}$	latent heat + sensible heat A
$_{lat,sen\ B}$	latent heat + sensible heat B
$_{m}$	melting
$_{next}$	next cell
$_{out}$	outlet condition
$_{ref}$	compared to the reference
$_{s_2}$	related to the solidified PCM thickness of the second cell
$_{s_{next}}$	related to the solidified PCM thickness of the next cell
$_{sol}$	solidification
$_{Stop}$	stop

Superscripts

^{air}	regarding air
^{cell}	with regard to one cell
^{init}	initial condition
^{LTES}	latent heat energy storage systems
$^{i-1}$	cell before
$^{i=2}$	2nd cell
^{water}	regarding water

CRediT authorship contribution statement

Andreas König-Haagen: Conceptualization, Methodology, Software, Validation, Investigation, Resources, Data Curation, Writing-Original draft preparation, Writing - Review & Editing, Visualization.

Gonzalo Diarce: Conceptualization, Methodology, Validation, Resources, Writing - Review & Editing.

Declaration of competing interest

The authors declare that they have no known competing financial interests or personal relationships that could have appeared to influence the work reported in this paper.

Data availability

Data will be made available on request.

Acknowledgments

Andreas König-Haagen is grateful for the financial support of the Deutsche Forschungsgemeinschaft, (DFG, German Research Foundation) under Grant no KO 6286/1-1 / 444616738.

This research was also funded by the Spanish Ministry of Science and Innovation (MICINN) through the STES4D research project (TED2021-131061B-C32).

Appendix A

In this section, the derivation from Eqs. (4) to (5) and eventually to Eq. (6) is shown. We start with calculating the solidification time of the second cell $t_{sol}^{i=2}$ by dividing it into two parts. The first part accounts for the time until s_{next} is solidified. This time equals t_{sol}^{init}. The second part is the time needed to solidify the rest. Since, after t_{sol}^{init}, the inlet temperature for the second cell is T_{in} (due to the assumption that there is no heat transfer within a cell once the cell has solidified), the time of the second part can be calculated by subtracting the time needed to solidify the cell until s_{next} (with T_{in} as inlet

temperature) from t_{sol}^{init}. This leads to Eq. (A1):

$$t_{sol}^{i=2} = t_{init} + \frac{s^2}{2 \bullet \lambda} \bullet L \bullet \rho \bullet s \bullet \frac{1}{T_m - T_{in}} - \frac{s_{next}^{i=2\,2}}{2 \bullet \lambda} \bullet L \bullet \rho \bullet s_{next} \bullet \frac{1}{T_m - T_{in}} \tag{A1}$$

Rearranging Eq. (A1) and writing it in a general form for every cell gives Eq. (A2):

$$t_{sol} = t_{sol}^{i-1} + \left(s^2 - s_{next}^{i=2\,2}\right) \bullet \left(\frac{1}{2 \bullet \lambda} \bullet L \bullet \rho \bullet \frac{1}{T_m - T_{in}}\right) \tag{A2}$$

Finally, inserting t_{sol}^{init} into Eq. (A2) allows it to be written in a compact form (see Eq. (5)). In conclusion, the solidification time of the second cell can be calculated by Eq. (A3):

$$t_{sol}^{i=2} = t_{sol}^{init} + \frac{s^2 - s_{next}^{i=2\,2}}{s^2} \bullet t_{sol}^{init}, \tag{A3}$$

$s_{next}^{i=2}$ can be calculated by Eq. (A4):

$$s_{next}^{i=2} = \sqrt{2 \bullet \frac{\lambda \bullet \left(T_m - \overline{T_{out}^{i=1}}\right)}{L \bullet \rho}} \bullet t_{sol}^{init} \tag{A4}$$

and $s_{next}^{i=3}$ can be calculated by Eq. (A5):

$$s_{next}^{i=3} = \sqrt{2 \bullet \frac{\lambda \bullet \left(T_m - \overline{T_{out}^{i=2}}\right)}{L \bullet \rho}} \bullet t_{sol}^{i=2} \tag{A5}$$

It is interesting to note that (Eq. (A6))

$$\left(T_m - \overline{T_{out}^{i=1}}\right) \bullet t_{sol}^{init} = \left(T_m - \overline{T_{out}^{i=2}}\right) \bullet t_{sol}^{i=2} \tag{A6}$$

as the heat transferred to every cell is identical after solidification and we then have (Eq. (A7))

$$Q = \left(T_m - \overline{T_{out}^{i-1}}\right) \bullet t_{sol}^{i-1} \bullet UA. \tag{A7}$$

According to Eqs. (A4) to (A6), it is also true that $s_{next}^{i=2} = s_{next}^{i=3}$ and, in consequence, we have (Eq. (A8))

$$t_{sol}^{i=2} - t_{sol}^{init} = t_{sol}^{i=3} - t_{sol}^{i=2}. \tag{A8}$$

It can also be shown that s_{next} is identical for all cells and, therefore, $t_{sol}^{i} - t_{sol}^{i-1}$ is identical for all cells as well. An illustrative explanation of this statement is that a part of the LHTESS can be defined as a new LHTESS. This new LHTESS includes all cells except for the first one. It is clear that the t_{sol}^{init} of this LHTESS equals the $t_{sol}^{i=2}$ of the original one. Now, Eq. (A8) can be applied to show that $t_{sol}^{i=3} - t_{sol}^{i=2} = t_{sol}^{i=4} - t_{sol}^{i=3}$ holds for the original LHTESS and the process can be repeated until the end of the LHTESS is reached. This explains why $t_{sol}^{i} - t_{sol}^{i-1}$ and s_{next} stay constant throughout all the cells of the LHTESS. Therefore, the solidification time can be calculated by Eq. (A9):

$$t_{sol}^{LTES} = t_{sol}^{init} + \left(t_{sol}^{i=2} - t_{sol}^{init}\right) \bullet n_{cell} \tag{A9}$$

Next, Eq. (A9) can be reformulated to find an independent solution of the number of cells n_{cell}. First, Eq. (A3) is used to replace $t_{sol}^{i=2}$ in Eq. (A9), which leads to Eq. (A10):

$$t_{sol}^{LTES} = t_{sol}^{init} + \left(t_{sol}^{init} + \frac{s^2 - s_{next}^{i=2\,2}}{s^2} \bullet t_{sol}^{init} - t_{sol}^{init}\right) \bullet n_{cell} \tag{A10}$$

Reformulating Eq. (A10) gives Eq. (A11):

$$t_{sol}^{LTES} = \left(1 + \frac{s^2 - s_{next}^{i=2\,2}}{s^2} \bullet n_{cell}\right) \bullet t_{sol}^{init} \tag{A11}$$

By replacing $s_{next}^{i=2}$ with $s \bullet \left[\left(T_m - \overline{T_{out}^{i=1}}\right)/\left(T_m - T_{in}\right)\right]^{1/2}$ and t_{sol}^{init} with the reformulated Eq. (A7) for the specific case of $\overline{T_{out}^{i-1}} = T_{in}$, we have Eq. (A12):

$$t_{sol}^{LTES} = \left(1 + \frac{s^2 - \left\{s \bullet \left[\frac{T_m - \overline{T_{out}^{i=1}}}{T_m - T_{in}}\right]^{1/2}\right\}^2}{s^2} \bullet n_{cell}\right) \bullet \frac{Q}{UA \bullet \left(T_m - T_{in}\right)} \tag{A12}$$

Reformulating Eq. (A12) leads to Eq. (A13):

$$t_{sol}^{LTES} = \left(1 + \left[1 - \frac{T_m - \overline{T_{out}^{i=1}}}{T_m - T_{in}}\right] \bullet n_{cell}\right) \bullet \frac{Q}{UA \bullet \left(T_m - T_{in}\right)} \tag{A13}$$

The next step is to insert the following expression for $\overline{T_{out}^{i=1}}$ (Eq. (A14))

$$\overline{T_{out}^{i=1}} = T_{in} + \frac{UA \bullet (T_m - T_{in})}{\dot{m} \bullet c_p \bullet n_{cell}} \tag{A14}$$

into Eq. (A13), resulting in Eq. (A15):

$$t_{sol}^{LTES} = \left(1 + \left[1 - \frac{\left(T_m - T_{in} - \frac{UA \bullet (T_m - T_{in})}{\dot{m} \bullet c_p \bullet n_{cell}}\right)}{(T_m - T_{in})}\right] \bullet n_{cell}\right) \bullet \frac{Q}{UA \bullet (T_m - T_{in})} \tag{A15}$$

Rearranging Eq. (A15) gives Eq. (A16):

$$t_{sol}^{LTES} = \left(1 + \left[1 - 1 + \frac{UA \bullet (T_m - T_{in})}{\dot{m} \bullet c_p \bullet n_{cell} \bullet (T_m - T_{in})}\right] \bullet n_{cell}\right) \bullet \frac{Q}{UA \bullet (T_m - T_{in})} \tag{A16}$$

Finally, simplifying Eq. (A16) further leads to Eq. (6).

Appendix B

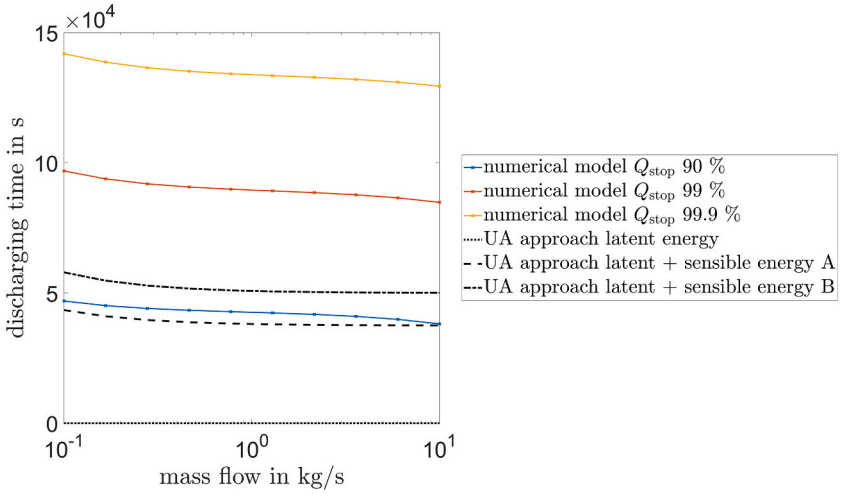

Fig. B1. Reference solution and predicted discharging times for the UA approach 1a for $\lambda = 0.1\mathrm{W/(mK)}$, $c = 2000\mathrm{J/(kgK)}$, $k = 1000\mathrm{W/(m^2K)}$ and $L = 1\mathrm{J/kg}$ (yields $Ste = 40000$ and $Bi = 500$).

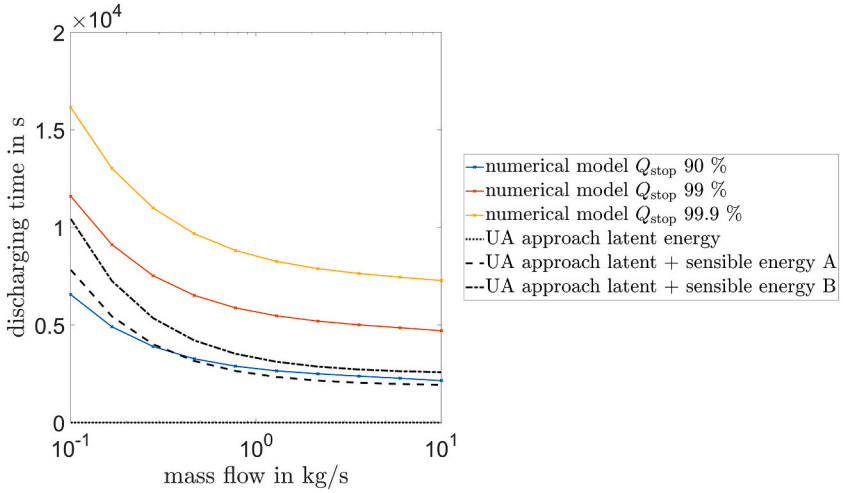

Fig. B2. Reference solution and predicted discharging times for the UA approach 1a for $\lambda = 2.0\mathrm{W/(mK)}$, $c = 2000\mathrm{J/(kgK)}$, $k = 1000\mathrm{W/(m^2K)}$ and $L = 1\mathrm{J/kg}$ (yields $Ste = 40000$ and $Bi = 25$).

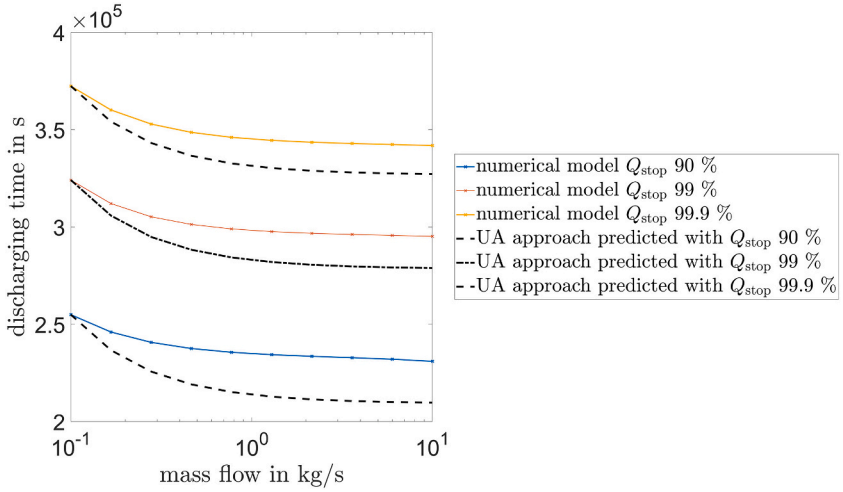

Fig. B3. Reference solution and predicted discharging times based on results with $\dot{m} = 0.1kg/s$ for the UA approach 1b for $\lambda = 0.1\mathrm{W/(mK)}$, $c = 2000\mathrm{J/(kgK)}$, $k = 1000\mathrm{W/(m^2K)}$ and $L = 200000\mathrm{J/kg}$ (yields $Ste = 0.2$ and $Bi = 500$).

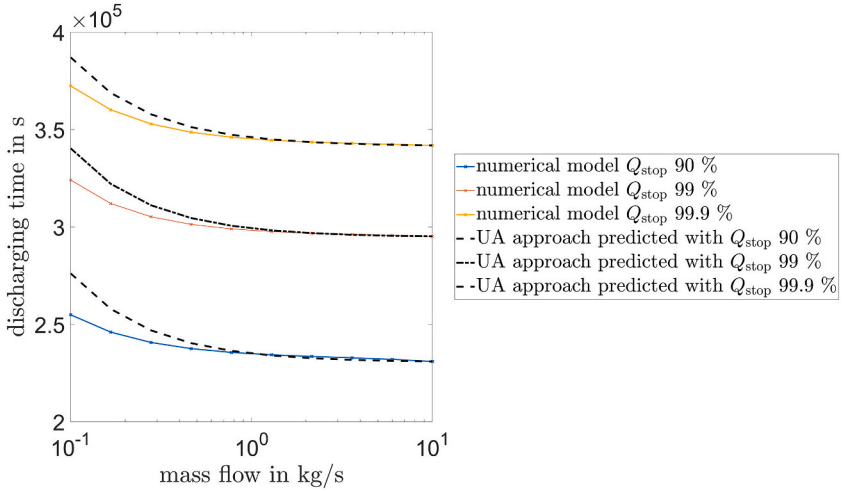

Fig. B4. Reference solution and predicted discharging times based on results with $\dot{m} = 10kg/s$ for the UA approach 1b for $\lambda = 0.1\mathrm{W/(mK)}$, $c = 2000\mathrm{J/(kgK)}$, $k = 1000\mathrm{W/(m^2K)}$ and $L = 200000\mathrm{J/kg}$ (yields $Ste = 0.2$ and $Bi = 500$).

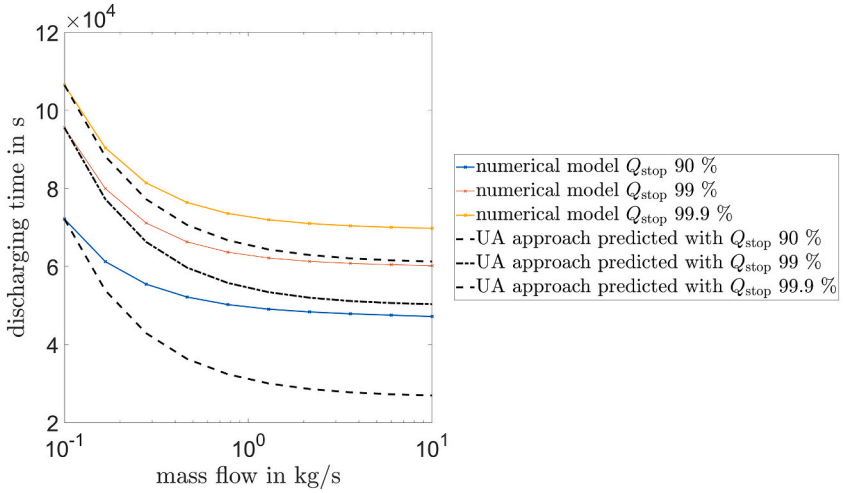

Fig. B5. Reference solution and predicted discharging times based on results with $\dot{m} = 0.1kg/s$ for the UA approach 1b for $\lambda = 0.5\mathrm{W/(mK)}$, $c = 2000\mathrm{J/(kgK)}$, $k = 1000\mathrm{W/(m^2K)}$ and $L = 200000\mathrm{J/kg}$ (yields $Ste = 0.2$ and $Bi = 100$).

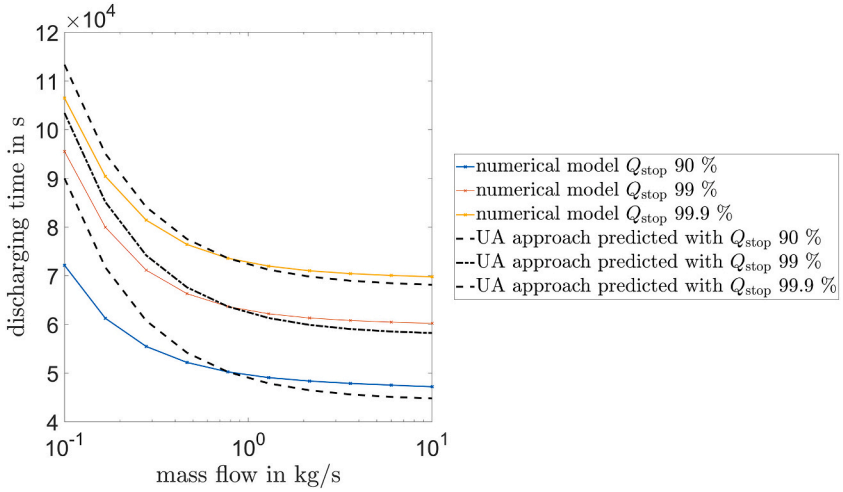

Fig. B6. Reference solution and predicted discharging times based on results with $\dot{m} = 0.7743 kg/s$ for the UA approach 1b for $\lambda = 0.5\mathrm{W/(mK)}$, $c = 2000\mathrm{J/(kgK)}$, $k = 1000\mathrm{W/(m^2K)}$ and $L = 200000\mathrm{J/kg}$ (yields $Ste = 0.2$ and $Bi = 100$).

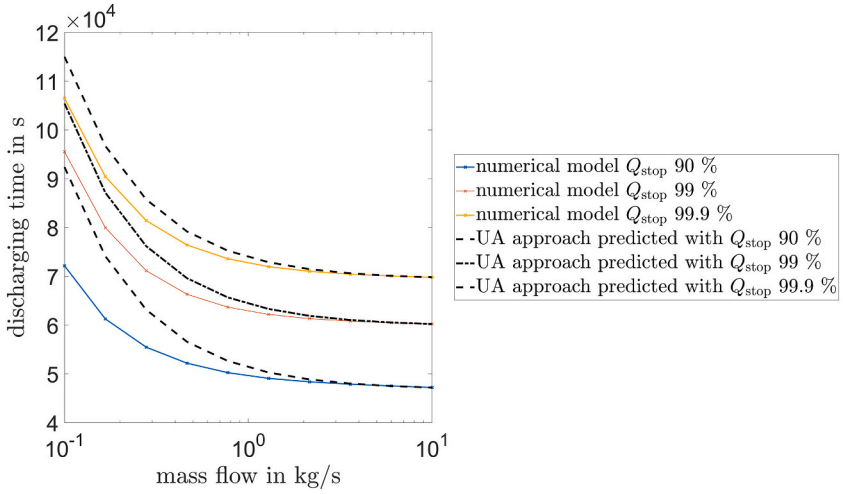

Fig. B7. Reference solution and predicted discharging times based on results with $\dot{m} = 10 kg/s$ for the UA approach 1b for $\lambda = 0.5\mathrm{W/(mK)}$, $c = 2000\mathrm{J/(kgK)}$, $k = 1000\mathrm{W/(m^2K)}$ and $L = 200000\mathrm{J/kg}$ (yields $Ste = 0.2$ and $Bi = 100$).

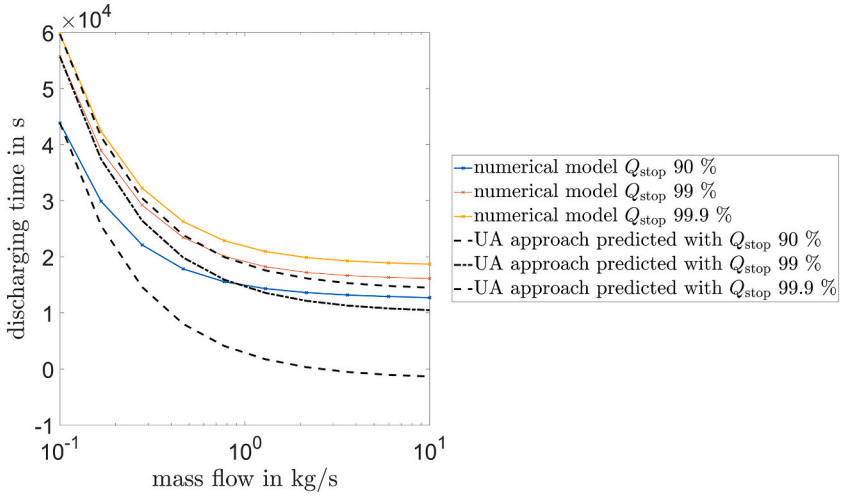

Fig. B8. Reference solution and predicted discharging times based on results with $\dot{m} = 0.1 kg/s$ for the UA approach 1b for $\lambda = 2.0\mathrm{W/(mK)}$, $c = 2000\mathrm{J/(kgK)}$, $k = 1000\mathrm{W/(m^2K)}$ and $L = 200000\mathrm{J/kg}$ (yields $Ste = 0.2$ and $Bi = 25$).

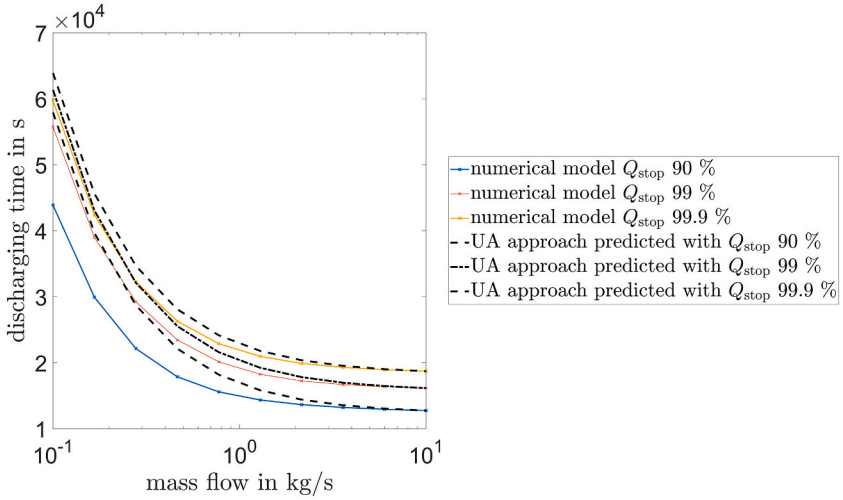

Fig. B9. Reference solution and predicted discharging times based on results with $\dot{m} = 10kg/s$ for the UA approach 1b for $\lambda = 2.0\text{W}/(\text{mK})$, $c = 2000\text{J}/(\text{kgK})$, $k = 1000\text{W}/(\text{m}^2\text{K})$ and $L = 200000\text{J}/\text{kg}$ (yields $Ste = 0.2$ and $Bi = 25$).

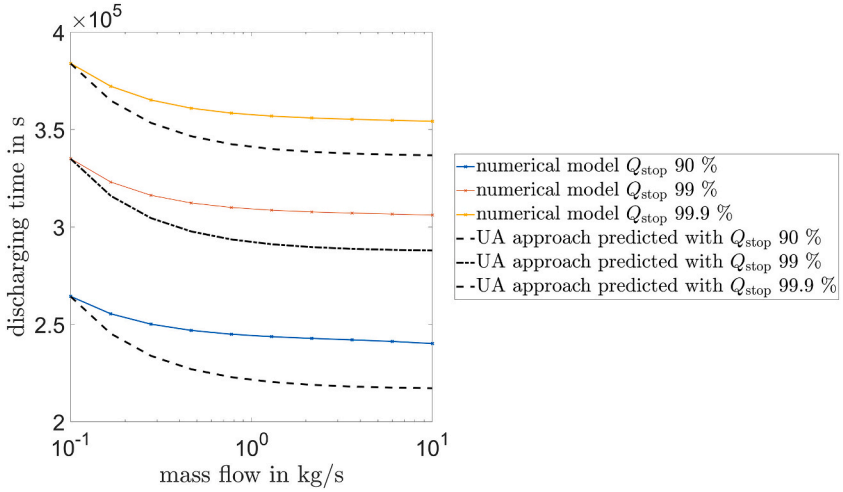

Fig. B10. Reference solution and predicted discharging times based on results with $\dot{m} = 0.1kg/s$ for the UA approach 2b for $\lambda = 0.1\text{W}/(\text{mK})$, $c = 2000\text{J}/(\text{kgK})$, $k = 100\text{W}/(\text{m}^2\text{K})$ and $L = 200000\text{J}/\text{kg}$ (yields $Ste = 0.2$ and $Bi = 50$).

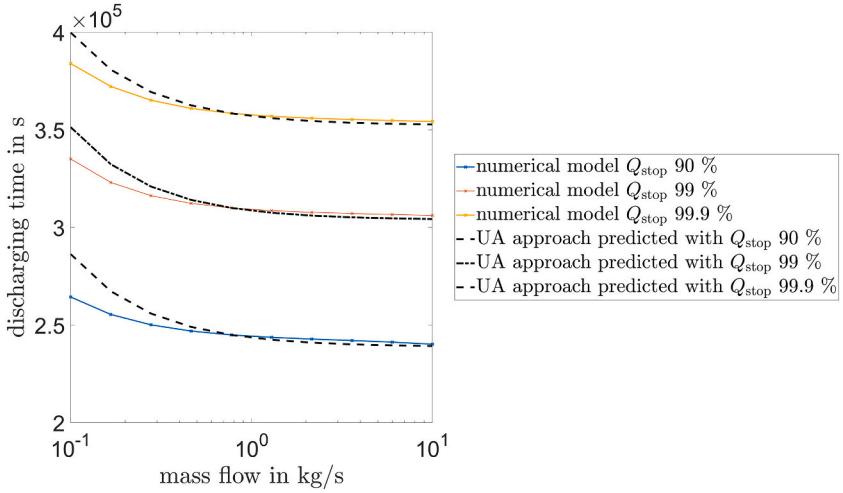

Fig. B11. Reference solution and predicted discharging times based on results with $\dot{m} = 0.7743kg/s$ for the UA approach 2b for $\lambda = 0.1\text{W}/(\text{mK})$, $c = 2000\text{J}/(\text{kgK})$, $k = 100\text{W}/(\text{m}^2\text{K})$ and $L = 200000\text{J}/\text{kg}$ (yields $Ste = 0.2$ and $Bi = 50$).

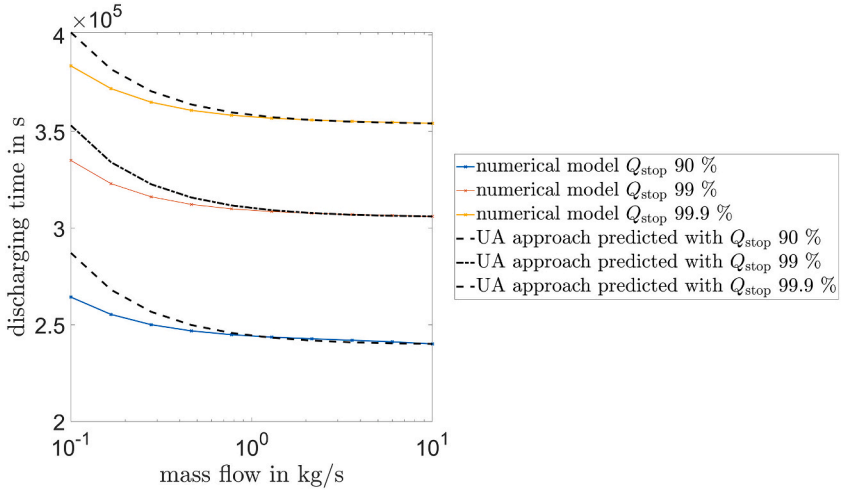

Fig. B12. Reference solution and predicted discharging times based on results with $\dot{m} = 10kg/s$ for the UA approach 2b for $\lambda = 0.1\mathrm{W/(mK)}$, $c = 2000\mathrm{J/(kgK)}$, $k = 100\mathrm{W/(m^2K)}$ and $L = 200000\mathrm{J/kg}$ (yields $Ste = 0.2$ and $Bi = 50$).

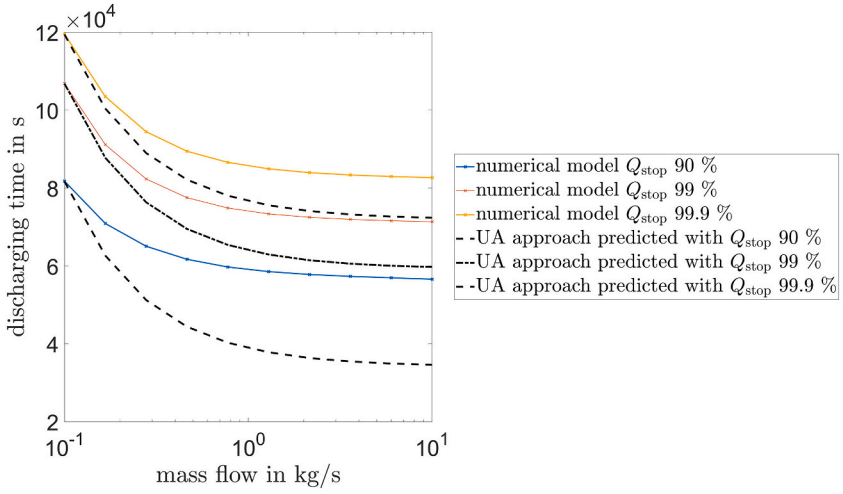

Fig. B13. Reference solution and predicted discharging times based on results with $\dot{m} = 0.1kg/s$ for the UA approach 2b for $\lambda = 0.5\mathrm{W/(mK)}$, $c = 2000\mathrm{J/(kgK)}$, $k = 100\mathrm{W/(m^2K)}$ and $L = 200000\mathrm{J/kg}$ (yields $Ste = 0.2$ and $Bi = 10$).

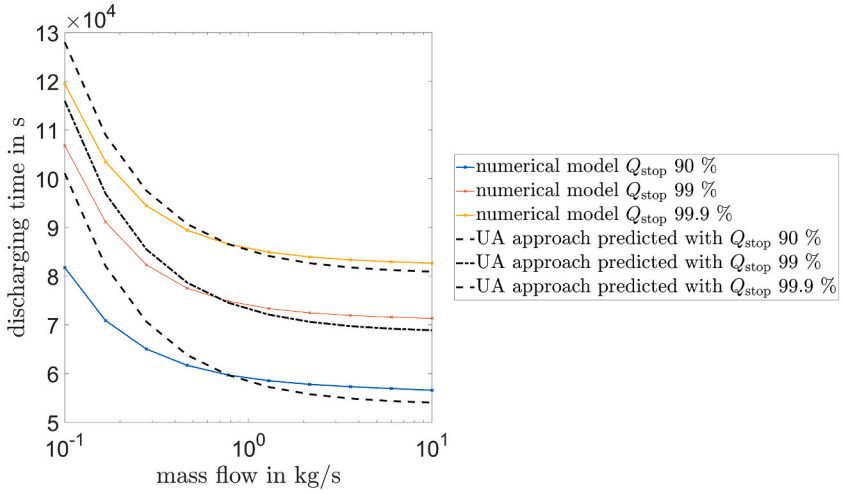

Fig. B14. Reference solution and predicted discharging times based on results with $\dot{m} = 0.7743kg/s$ for the UA approach 2b for $\lambda = 0.5\mathrm{W/(mK)}$, $c = 2000\mathrm{J/(kgK)}$, $k = 100\mathrm{W/(m^2K)}$ and $L = 200000\mathrm{J/kg}$ (yields $Ste = 0.2$ and $Bi = 10$).

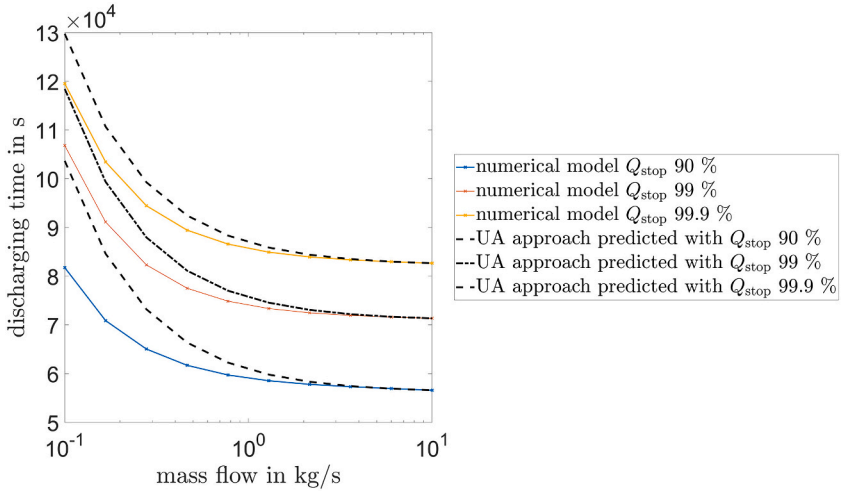

Fig. B15. Reference solution and predicted discharging times based on results with $\dot{m} = 10kg/s$ for the UA approach 2b for $\lambda = 0.5\text{W}/(\text{mK})$, $c = 2000\text{J}/(\text{kgK})$, $k = 100\text{W}/(\text{m}^2\text{K})$ and $L = 200000\text{J}/\text{kg}$ (yields $Ste = 0.2$ and $Bi = 10$).

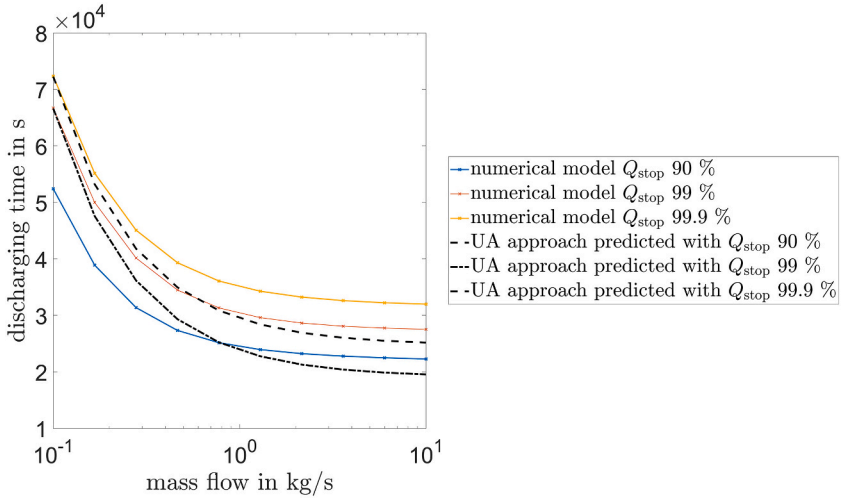

Fig. B16. Reference solution and predicted discharging times based on results with $\dot{m} = 0.1kg/s$ for the UA approach 2b for $\lambda = 2.0\text{W}/(\text{mK})$, $c = 2000\text{J}/(\text{kgK})$, $k = 100\text{W}/(\text{m}^2\text{K})$ and $L = 200000\text{J}/\text{kg}$ (yields $Ste = 0.2$ and $Bi = 2.5$).

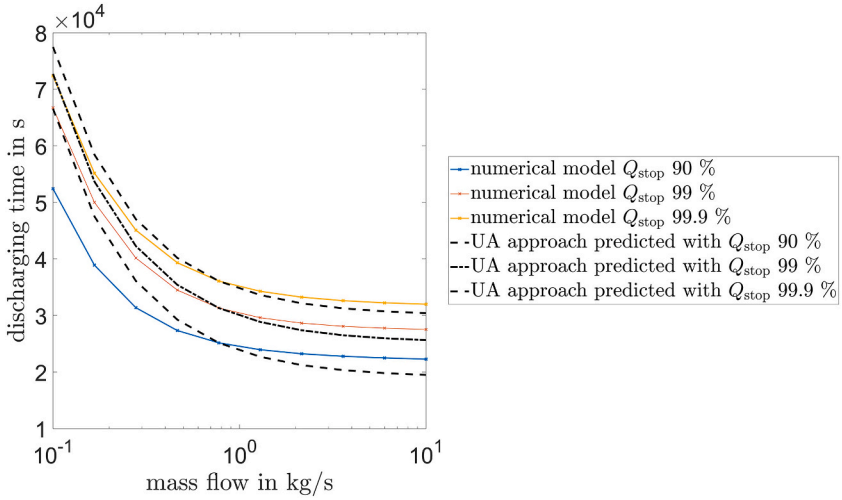

Fig. B17. Reference solution and predicted discharging times based on results with $\dot{m} = 0.7743kg/s$ for the UA approach 2b for $\lambda = 2.0\text{W}/(\text{mK})$, $c = 2000\text{J}/(\text{kgK})$, $k = 100\text{W}/(\text{m}^2\text{K})$ and $L = 200000\text{J}/\text{kg}$ (yields $Ste = 0.2$ and $Bi = 2.5$).

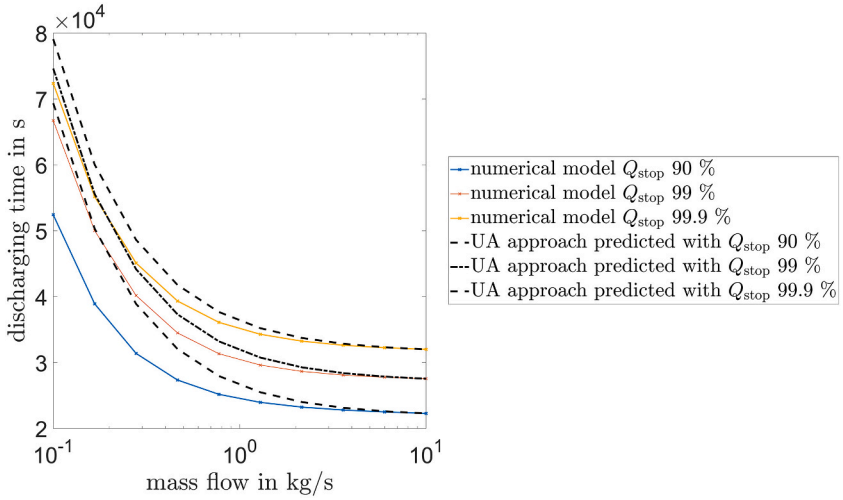

Fig. B18. Reference solution and predicted discharging times based on results with $\dot{m} = 10kg/s$ for the UA approach 2b for $\lambda = 2.0\mathrm{W/(mK)}$, $c = 2000\mathrm{J/(kgK)}$, $k = 100\mathrm{W/(m^2K)}$ and $L = 200000\mathrm{J/kg}$ (yields $Ste = 0.2$ and $Bi = 2.5$).

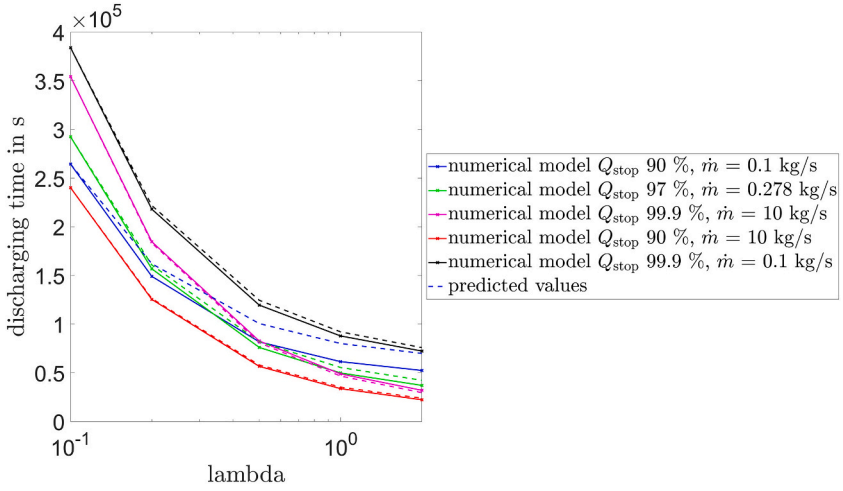

Fig. B19. Reference solution and predicted discharging times based on results with $\lambda = 0.1\mathrm{W/(mK)}$ for the UA approach 2b for $c = 2000\mathrm{J/(kgK)}$, $k = 100\mathrm{W/(m^2K)}$ and $L = 200000\mathrm{J/kg}$ (yields $Ste = 0.2$).

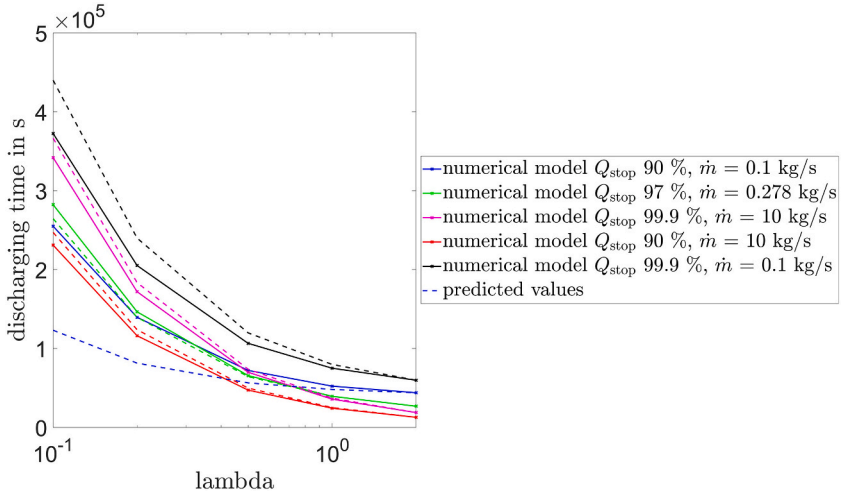

Fig. B20. Reference solution and predicted discharging times based on results with $\lambda = 2.0\mathrm{W/(mK)}$ for the UA approach 2b for $c = 2000\mathrm{J/(kgK)}$, $k = 100\mathrm{W/(m^2K)}$ and $L = 200000\mathrm{J/kg}$ (yields $Ste = 0.2$).

Table C 1
Mean deviation of t_{sol}^{LTES} between the reference solution and the UA approaches 1a and 2a. The relative variation of t_{sol}^{LTES} of the reference solution Δt_{ref} is given as a reference.

	c	L	λ	k	$Q_{Stop} = 90\,\%$				$Q_{Stop} = 99\,\%$				$Q_{Stop} = 99.9\,\%$			
Figure	J/(kgK)	kJ/kg	W/(mK)	W/(m^{2}K)	$\bar{\varepsilon}_L$	$\bar{\varepsilon}_{L+sen\,A}$	$\bar{\varepsilon}_{L+sen\,B}$	Δt_{ref}	$\bar{\varepsilon}_L$	$\bar{\varepsilon}_{L+sen\,A}$	$\bar{\varepsilon}_{L+sen\,B}$	Δt_{ref}	$\bar{\varepsilon}_L$	$\bar{\varepsilon}_{L+sen\,A}$	$\bar{\varepsilon}_{L+sen\,B}$	Δt_{ref}
3	200	200	0.1	1000	24.08	25.95	26.57	9.51	2.19	3.73	4.24	9.39	0.94	0.72	1.18	11.71
4	200	200	2.0	1000	25.62	27.50	28.13	71.66	3.49	3.84	3.96	72.75	4.98	3.56	3.20	73.65
5 (no HTF)	200	200	2.0	1000	69.24	70.58	71.03	95.91	33.44	32.44	32.11	90.53	39.65	38.75	38.44	90.68
5 (HTF)	200	200	2.0	1000	89.11	91.17	91.85	95.91	2.33	2.80	2.95	90.53	10.08	9.17	8.87	90.68
6 (no conv)	200	200	2.0	100	20.45	19.86	19.71	57.95	31.19	30.15	29.81	61.07	34.45	33.47	33.14	62.44
6 (conv)	200	200	2.0	100	26.07	27.96	28.59	57.95	4.41	5.98	6.50	61.07	0.71	1.22	1.63	62.44
7	2000	200	0.1	1000	9.21	25.60	31.06	9.40	14.08	1.93	3.11	8.93	25.69	14.54	10.83	8.20
8	2000	200	2.0	1000	11.25	27.94	33.50	70.98	13.34	5.18	5.90	71.02	23.12	11.69	9.27	68.68
B1	2000	0	0.1	1000	100.00	8.33	22.22	18.71	100.00	56.70	42.27	12.47	100.00	71.04	61.38	8.79
B2	2000	0	2.0	1000	100.00	10.82	27.77	67.23	100.00	51.96	35.94	59.40	100.00	67.53	56.70	54.92

Table C 2
Mean deviation of t_{sol}^{LTES} between the reference solution and the UA approaches 1b and 2b for predicting t_{sol}^{LTES} for different $\dot{m}$. The relative variation of t_{sol}^{LTES} of the reference solution Δt_{ref} is given as a reference.

Figure	UA version	c	L	λ	k	$\dot{m}$ (based on)	$Q_{Stop} = 90\,\%$		$Q_{Stop} = 99\,\%$		$Q_{Stop} = 99.9\,\%$	
		J/(kgK)	kJ/kg	W/(mK)	W/(m^{2}K)	kg/s	$\bar{\varepsilon}$	Δt_{ref}	$\bar{\varepsilon}$	Δt_{ref}	$\bar{\varepsilon}$	Δt_{ref}
B3	1b	2000	200	0.1	1000	0.1	7.34	9.40	4.19	8.93	3.31	8.20
9	1b	2000	200	0.1	1000	0.7743	1.86	9.40	1.18	8.93	0.89	8.20
B4	1b	2000	200	0.1	1000	10	1.86	9.40	1.22	8.93	0.91	8.20
B5	1b	2000	200	0.5	1000	0.1	30.79	34.60	11.03	36.97	8.25	34.46
B6	1b	2000	200	0.5	1000	0.7743	7.64	34.60	3.41	36.97	2.58	34.46
B7	1b	2000	200	0.5	1000	10	7.98	34.60	3.77	36.97	2.83	34.46
B8	1b	2000	200	2.0	1000	0.1	68.46	70.98	20.54	71.02	12.90	68.68
10	1b	2000	200	2.0	1000	0.7743	15.53	70.98	5.38	71.02	3.95	68.68
B9	1b	2000	200	2.0	1000	10	15.40	70.98	5.76	71.02	4.25	68.68
B10	2b	2000	200	0.1	100	0.1	7.63	9.16	4.53	8.65	3.81	7.74
B11	2b	2000	200	0.1	100	0.7743	1.93	9.16	1.26	8.65	1.01	7.74
B12	2b	2000	200	0.1	100	10	1.92	9.16	1.30	8.65	1.03	7.74
B13	2b	2000	200	0.5	100	0.1	28.17	30.79	11.17	33.21	8.67	30.83
B14	2b	2000	200	0.5	100	0.7743	7.05	30.79	3.48	33.21	2.56	30.83
B15	2b	2000	200	0.5	100	10	7.39	30.79	3.72	33.21	2.79	30.83
B16	2b	2000	200	2.0	100	0.1	-	57.49	18.28	58.72	13.49	55.77
B17	2b	2000	200	2.0	100	0.7743	12.04	57.49	5.02	58.72	3.86	55.77
B18	2b	2000	200	2.0	100	10	12.54	57.49	5.44	58.72	4.15	55.77

Table C 3
Mean deviation of t_{sol}^{LTES} between the reference solution and the UA approaches 1b and 2b for predicting t_{sol}^{LTES} for different λ. The relative variation of t_{sol}^{LTES} of the reference solution Δt_{ref} is given as a reference.

Figure	UA version	c	L	λ	k	$Q_{Stop} = 90\,\%$ $\dot{m} = 0.1$ kg/s		$Q_{Stop} = 97\,\%$ $\dot{m} = 0.278$ kg/s		$Q_{Stop} = 99.9\,\%$ $\dot{m} = 10$ kg/s		$Q_{Stop} = 90\,\%$ $\dot{m} = 10$ kg/s		$Q_{Stop} = 99.9\,\%$ $\dot{m} = 0.1$ kg/s	
		J/(kgK)	kJ/kg	W/(mK)	W/(m^{2}K)	$\bar{\varepsilon}$	Δt_{ref}	$\bar{\varepsilon}$	Δt_{ref}	$\bar{\varepsilon}$	Δt_{ref}	$\bar{\varepsilon}$	Δt_{ref}	$\bar{\varepsilon}$	Δt_{ref}
11	1b	2000	200	0.1	1000	18.93	82.79	6.66	90.51	2.25	94.53	2.06	94.49	4.34	83.97
12	1b	2000	200	2.0	1000	64.94	82.79	13.89	90.51	4.31	94.53	4.07	94.49	10.63	83.97
B19	2b	2000	200	0.1	100	19.07	80.17	7.08	87.32	3.00	90.97	2.98	90.72	3.10	81.16
B20	2b	2000	200	2.0	100	-	80.17	19.15	87.32	8.27	90.97	7.71	90.72	8.64	81.16

References

[1] M.M. Farid, A.M. Khudhair, S.A.K. Razack, S. Al-Hallaj, A review on phase change energy storage: materials and applications, Energy Convers. Manag. 45 (2004) 1597–1615, https://doi.org/10.1016/j.enconman.2003.09.015.

[2] D. Groulx, The rate problem in solid-liquid phase change heat transfer: efforts and questions toward heat exchanger design rules, in: Proceedings of the 16th International Heat Transfer Conference, 16th International Heat Transfer Conference, Beijing, China, August 10-15, 2018, 2018.

[3] S. Jegadheeswaran, S.D. Pohekar, Performance enhancement in latent heat thermal storage system: a review, Renew. Sust. Energ. Rev. 13 (2009) 2225–2244.

[4] S. Jegadheeswaran, A. Sundaramahalingam, S.D. Pohekar, Alternative heat transfer enhancement techniques for latent heat thermal energy storage system: a review, Int. J. Thermophys. 42 (2021) 1–48, https://doi.org/10.1007/s10765-021-02921-x.

[5] A. König-Haagen, S. Höhlein, A. Lázaro, M. Delgado, G. Diarce, D. Groulx, F. Herbinger, A. Patil, G. Englmair, G. Wang, et al., Analysis of the discharging process of latent heat thermal energy storage units by means of normalized power parameters, J. Energy Storage 72 (2023), 108428, https://doi.org/10.1016/j.est.2023.108428.
[6] L. Kalapala, J.K. Devanuri, Influence of operational and design parameters on the performance of a PCM based heat exchanger for thermal energy storage – a review, J. Energy Storage 20 (2018) 497–519, https://doi.org/10.1016/j.est.2018.10.024.
[7] A. Lázaro, M. Delgado, A. König-Haagen, S. Höhlein, G. Diarce, Technical performance assessment of phase change material components, in: SHC 2019 International Conference on Solar Heating and Cooling for Building and Industry, Santiago de Chile, Chile, 4-7 November 2019, 2019.
[8] B.D. Mselle, G. Zsembinszki, D. Vérez, E. Borri, L.F. Cabeza, A detailed energy analysis of a novel evaporator with latent thermal energy storage ability, Appl. Therm. Eng. 201 (2022), 117844, https://doi.org/10.1016/j.applthermaleng.2021.117844.
[9] G. Lamé, B.P. Clapeyron, Mémoire sur la solidification par refroidissement d'un globe solide, Ann. Chim. Phys. 47 (1831) 250–256.
[10] J. Stefan, Uber einige probleme der theorie der warmeletung, Sitzungsber. Akad. Wiss. Wien, Math.-Naturwiss. 98 (1889) 473–484.
[11] D. Tarzia, in: M. El-Amin (Ed.), Explicit and Approximated Solutions for Heat and Mass Transfer Problems With a Moving Interface, Advanced Topics in Mass Transfer, InTech, 2011. ISBN 978-953-307-333-0.
[12] V. Alexiades, A.D. Solomon, Mathematical Modeling of Melting and Freezing Processes, Hemisphere Pub. Corp., Washington, 1993. ISBN 9781560321255.
[13] A. Bejan, Single correlation for theoretical contact melting results in various geometries, Int. Commun. Heat Mass Transf. 19 (1992) 473–483, https://doi.org/10.1016/0735-1933(92)90003-Z.
[14] D. Groulx, M. Lacroix, Study of the effect of convection on close contact melting of high Prandtl number substances, Int. J. Therm. Sci. 46 (2007) 213–220, https://doi.org/10.1016/j.ijthermalsci.2006.04.017.
[15] C. Beckermann, A general correlation for melting in rectangular enclosures, J. Heat Transf. 1111–1115 (1989).
[16] T. Hirata, Y. Makino, Y. Kaneko, Analysis of close-contact melting for octadecane and ice inside isothermally heated horizontal rectangular capsule, Int. J. Heat Mass Transf. 34 (1991) 3097–3106, https://doi.org/10.1016/0017-9310(91)90079-T.
[17] M.K. Moallemi, B.W. Webb, R. Viskanta, An experimental and analytical study of close-contact melting, J. Heat Transf. 108 (1986) 894, https://doi.org/10.1115/1.3247030.
[18] G. Diarce, Á. Campos-Celador, L. Quant, A.M. García-Romero, A novel correlation for the direct determination of the discharging time of plate-based latent heat thermal energy storage systems, Appl. Therm. Eng. 129 (2018) 521–534, https://doi.org/10.1016/j.applthermaleng.2017.10.057.
[19] K. Ismail, M.M. Gonçalves, Thermal performance of a pcm storage unit, Energy Convers. Manag. 40 (1999) 115–138, https://doi.org/10.1016/S0196-8904(98)00042-9.
[20] N. Amin, F. Bruno, M. Belusko, Effectiveness–NTU correlation for low temperature PCM encapsulated in spheres, Appl. Energy 93 (2012) 549–555, https://doi.org/10.1016/j.apenergy.2011.12.006.
[21] N. Amin, M. Belusko, F. Bruno, An effectiveness-NTU model of a packed bed PCM thermal storage system, Appl. Energy 134 (2014) 356–362, https://doi.org/10.1016/j.apenergy.2014.08.020.
[22] N.H. Tay, M. Belusko, F. Bruno, An effectiveness-NTU technique for characterising tube-in-tank phase change thermal energy storage systems, Appl. Energy 91 (2012) 309–319.
[23] M. Belusko, E. Halawa, F. Bruno, Characterising PCM thermal storage systems using the effectiveness-NTU approach, Int. J. Heat Mass Transf. 55 (2012) 3359–3365.
[24] M. Bechiri, K. Mansouri, Exact solution of thermal energy storage system using PCM flat slabs configuration, Energy Convers. Manag. 76 (2013) 588–598.
[25] C. Ding, Z. Niu, B. Li, D. Hong, Z. Zhang, M. Yu, Analytical modeling and thermal performance analysis of a flat plate latent heat storage unit, Appl. Therm. Eng. 179 (2020), 115722.
[26] R. Raud, M.E. Cholette, S. Riahi, F. Bruno, W. Saman, G. Will, T.A. Steinberg, Design optimization method for tube and fin latent heat thermal energy storage systems, Energy 134 (2017) 585–594.
[27] T. Bauer, Approximate analytical solutions for the solidification of PCMs in fin geometries using effective thermophysical properties, Int. J. Heat Mass Transf. 54 (2011) 4923–4930, https://doi.org/10.1016/j.ijheatmasstransfer.2011.07.004.
[28] W. Beyne, R. Tassenoy, M. de Paepe, An approximate analytical solution for the movement of the phase change front in latent thermal energy storage heat exchangers, J. Energy Storage 57 (2023), 106132.
[29] W. Beyne, I. T'Jollyn, S. Lecompte, L.F. Cabeza, M. de Paepe, Standardised methods for the determination of key performance indicators for thermal energy storage heat exchangers, Renew. Sust. Energ. Rev. 176 (2023), 113139.
[30] A. König-Haagen, G. Diarce, Comparison of corrected and uncorrected enthalpy methods for solving conduction-driven solid/liquid phase change problems, Energies 16 (2023) 449, https://doi.org/10.3390/en16010449.
[31] M. Griesbach, A. König-Haagen, D. Brüggemann, Numerical analysis of a combined heat pump ice energy storage system without solar benefit – analytical validation and comparison with long term experimental data over one year, Appl. Therm. Eng. 213 (2022), https://doi.org/10.1016/j.applthermaleng.2022.118696.
[32] J.A. Nelder, R. Mead, A simplex method for function minimization, Comput. J. 7 (1965) 308–313, https://doi.org/10.1093/comjnl/7.4.308.